Surface Plasmon Resonance (SPR) Refract metric Sensor with Au-TiO_2 Coated Photonic Crystal Fiber for Cancer Cell Detection

This paper has been submitted to the Department of Electrical & Electronic Engineering of the Canadian University of Bangladesh in partial fulfillment of the requirement for the degree of Bachelor of Science in Electrical and Electronic Engineering.

SUBMITTED BY:

Imtiaz Hussain	21108001
Md Akhlakur Rahman Ahad	21108008
Md Moniruzzaman	21208004

SUPERVISED BY:

Arnab Saha
Lecturer
Department of Electrical and Electronic Engineering

CANADIAN UNIVERSITY OF BANGLADESH

Letter of Transmittal

28th November 2024

To
The Supervisor
Department of EEE
Canadian University of Bangladesh
RANGS RL SQUARE, PRAGATI SHARAN,
Bir Uttam Rafiqul Islam Avenue Dhaka-1212.

Subject: **Submission of the Project report.**

Dear Sir,

Please find enclosed the project report entitled **"Surface Plasmon Resonance (SPR) Refractometric Sensor with Au-TiO_2 Coated Photonic Crystal Fiber for Cancer Cell Detection"**. The study has been carried out in partial fulfillment of the requirements for the degree of Bachelor of Science in Electrical & Electronics Engineering.

In carrying out the study, we followed the supervisor's advice and collected the required information from several textbooks, reference books, websites, and other sources. We think you will find it useful and informative. We would be glad to furnish you with further explanations or clarifications if required.

Sincerely yours,

_ _ _ _ _ _ _ _ _ _ _ _ _ _ _
Imtiaz Hussain
ID: 21108001

_ _ _ _ _ _ _ _ _ _ _ _ _ _ _
Md Akhlakur Rahman Ahad
ID: 21108008

_ _ _ _ _ _ _ _ _ _ _ _ _ _ _
Moniruzzaman
ID: 21208004

Declaration

We do Here solemnly declare that the work presented in this report entitled **"Surface Plasmon Resonance (SPR) Refractometric Sensor with Au-TiO_2 Coated Photonic Crystal Fiber for Cancer Cell Detection"** has been carried out by us and has not been previously submitted to any other university, college, or organization for an academic qualification, certificate or degree. We hereby warrant that the work that has been presented here does not breach any existing copyright. We further undertake to indemnify the university against any loss or damage arising from a breach of the foregoing obligations.

Authors

_ _ _ _ _ _ _ _ _ _ _ _ _ _ _

Imtiaz Hussain
ID: 21108001

_ _ _ _ _ _ _ _ _ _ _ _ _ _ _ _

Md Akhlakur Rahman Ahad
ID: 21108008

_ _ _ _ _ _ _ _ _ _ _ _ _ _ _ _

Moniruzzaman
ID: 21208004

CANADIAN UNIVERSITY OF BANGLADESH

Certificate

This is to certify that the report entitled '**Surface Plasmon Resonance (SPR) Refractometric Sensor with Au-TiO_2 Coated Photonic Crystal Fiber for Cancer Cell Detection'** is a valid record of the work done by **Imtiaz Hussain, Md Akhlakur Rahman Ahad** and **Md Moniruzzaman** for partial fulfillment of the requirement of the degree of B.Sc. in Electrical and Electronic Engineering (EEE) from the Canadian University of Bangladesh.

This work has been carried out under my guidance and is a confident record of valid works carried out successfully.

Faculty Guide

_ _ _ _ _ _ _ _ _ _ _ _ _ _ _ _ _ _ _ _

Arnab Saha
Lecturer
Department of Electrical and Electronic Engineering

Acknowledgment

We would like to express our greatest gratitude to the people who helped and supported us throughout this work. First and foremost, we would like to thank our honorable supervisor, **Arnab Saha**, Lecturer, Department of EEE, for giving us enormous support, advice and valued guidance concerning this thesis.

We are grateful to Professor **Ifat Al Baqee**, Honorable Department head of EEE, Faculty of Engineering, Canadian University of Bangladesh (CUB) for his comments, encouragement, and support.

We are grateful to our respected coordinator **Arnab Saha**, Lecturer, Department of EEE, Faculty of Engineering, Canadian University of Bangladesh (CUB) for kindly agreeing to examine our thesis.

Next, we would like to thank our family and friends for their valuable support in completing this thesis.

Finally, we would like to express our heartiest gratefulness to Almighty Allah for His heavenly blessings. Without his blessings, it would not be possible to complete our work successfully.

Thank you all

Authors

_ _ _ _ _ _ _ _ _ _ _ _ _ _

Imtiaz Hussain
ID: 21108001

_ _ _ _ _ _ _ _ _ _ _ _ _ _ _

Md Akhlakur Rahman Ahad
ID: 21108008

_ _ _ _ _ _ _ _ _ _ _ _ _ _

Md Moniruzzaman
ID: 21208004

Executive Summary

Cancer remains a leading cause of mortality worldwide, with specific types such as breast, adrenal gland, cervical, and blood cancers being prominent in clinical research due to their high incidence and unique biological characteristics. This summary focuses on five distinct cancer cell lines that represent these types, each contributing valuable insights into cancer behavior, treatment responses, and biomarker identification.

Breast cancer, one of the most common cancers in women, includes two widely studied cell lines: MDA-MB-231 and MCF7. MDA-MB-231, a model for triple-negative breast cancer (TNBC), lacks estrogen, progesterone, and HER2 receptors, making it more aggressive and resistant to hormone therapies. In contrast, MCF7 represents hormone receptor-positive breast cancer, with estrogen receptor positivity, making it responsive to hormonal therapies, thus reflecting a different therapeutic strategy and prognosis from TNBC. PC12, an adrenal gland cancer cell line derived from pheochromocytoma, models adrenal gland tumors that can affect hormonal balance and trigger complex symptoms. PC12 cells are particularly important for studying tumor neurobiology and testing novel treatments targeting neural pathways.

HeLa, a cell line from cervical cancer, is immortalized and has been used extensively in research due to its robustness and genetic stability. It has been pivotal in understanding human papillomavirus (HPV)-related cervical cancers, immune responses, and viral oncology.

Jurkat cells, derived from T-cell leukemia, represent blood cancer and are integral for studying T-cell signaling, apoptosis, and immunotherapy responses. This cell line has provided critical insights into leukemia pathology and advancements in CAR-T cell therapy.

Together, these cell lines enable targeted studies across different cancer types, supporting the development of novel diagnostics and therapeutic approaches, while advancing personalized treatment strategies for these diverse cancers. This summary highlights each cell line's characteristics, relevance, and role in cancer research, capturing the importance of each in advancing cancer diagnostics and therapeutics. Nowadays the home safety detection system plays an important role in the security of people.

Since all the people from home go to work daily, it is impossible to check on the appliances available at home especially different types of cancer cell detection Breast Cancer Type-1 MDA-MB231, Breast cancer Type-2 MCF7, Adrenal glands cancer PC12, Cervical cancer Hela, Blood cancer and Jurkat. whereas in the industrial system, it also makes it difficult for the laboratories to test to Hospital track of every second so to work on this problem, the system is developed which will keep track of various home appliances such as Breast Cancer Type-1 MDA-MB231, Breast cancer Type-2 MCF7, Adrenal glands cancer PC12, Cervical cancer Hela, Blood cancer and Jurkat sensor to detect. This summary highlights each cell line's characteristics, relevance, and role in cancer research, capturing the importance of each in advancing cancer diagnostics and therapeutics.

TABLE OF CONTENTS **Page**

LIST OF FIGURES

LIST OF TABLES

MATHEMATICAL TREM

CHAPTER 1 INTRODUCTION

1: Introduction

The term "cancer" refers to a broad range of illnesses that can impact any part of the body. About 10 million people died from cancer in 2020, making it the leading cause of death worldwide. In 2020, the most common causes of cancer-related deaths were breast, lung, liver, stomach, colon, and rectal cancer. The fast growth of aberrant cells that spread beyond their natural boundaries and have the potential to invade nearby organs and spread to other areas of the body is what causes cancer. Normal cells can change into cancerous cells, which is how cancer arises. Risk factors for cancer include air pollution, radiation, infections, poor dietary habits, alcohol use, tobacco use, and physical inactivity. [1], [2], [3], [4]. Early diagnosis and treatment can reduce the death rate from cancer. The conventional methods of diagnosing cancer include physical examinations, biopsies, endoscopic procedures, and X-rays; however, these technologies are expensive and require significant financial outlays. Therefore, quick and accurate cancer diagnosis methods are required. The application of SPR-based photonic crystal fiber (PCF) refractometric sensors for illness diagnostics is presently being studied in the biomedical field. The RI of the analyte materials and the outside factors governing the sensing property both have a significant impact on PCF sensitivity. Hydrostatic pressure [5], temperature [6], refractive index [7], magnetic field [8], strain [9], and other variables can all be sensed with PCFs. Toxic compounds [10], [11], cholesterol [12], DNA [13], and glucose [14] can also be detected using PCF-based chemicals and sensors. Several methods for identifying cancerous cells early on have been given in the research. Li et al. introduced an electrochemical method for identifying breast cancer [16], whereas Laszlo Hajba et al. suggest a microfluidic device for identifying tumor cells in the blood [15]. Immuno magnetic nanoparticles were used by Li et al. to identify breast cancer cells [17], and Liu et al. used Raman spectroscopy to identify cancerous cells [18]. The methods that are being discussed promise better results and higher sensitivity for early cancer detection. Instead of depending on viral treatment, Ayana et al. use PCF to assess the refractive index of cancer samples based on detection [19]. Malignancy can be found by putting a sample cell into the PCF's cavity. The number and size of cancer cells have little bearing on the PCF structure's ability to sense. However, the fluids from cancer cells and the transmitted optical source are the main emphasis. In order to diagnose breast cancer type-1, breast cancer type-2, adrenal glands, cervical, and

blood cancer, respectively, this research proposes a PCF that uses the SPR principle to recognize MDAMB-231, MCF-7, PC12, HeLa, and Jurkat malignant cells [3]. Liquid samples of malignant cells and their normal counterparts are taken into consideration at 80% and 30%–70% concentrations, respectively. The hypothesized cancer's wavelength sensitivity was determined using the finite element method (FEM) [37]. When the core guided mode is combined with the SPP guided mode, the resonance wavelength shift between the malignant and normal cells is measured to estimate the refractive sensor [12]. The amplitude sensitivity for identifying each malignant cell is also calculated using the amplitude interrogation technique. In order to identify any alterations in the sample cell's RI, the resolution of the suggested PCF is established [15]. The goal of this research is to quickly identify different types of malignant cells using a straightforward detection method.

1.1 Background on Cancer Detection:

Cancer detection is a crucial area in medical diagnostics, aiming to identify malignancies at an early stage to enhance treatment outcomes and survival rates. Current methods include imaging techniques like MRI, CT scans, and mammography, as well as molecular diagnostics, such as biopsies and biomarker-based blood tests [23]. These approaches, while effective, can sometimes be invasive, expensive, or require specialized infrastructure, limiting their accessibility. In recent years, Bio sensing technologies, particularly those utilizing surface plasmon resonance (SPR) [23], have gained attention for their potential in cancer detection. SPR-based sensors are non-invasive, highly sensitive, and capable of real-time detection of molecular interactions [28]. They work by detecting refractive index changes at the interface between a metal surface and a sample medium, making them ideal for identifying cancer biomarkers in biological fluids [25]. Advancements in photonic crystal fiber (PCF)-based SPR sensors, coupled with materials like gold and titanium dioxide (Au-TiO_2) [22], have further enhanced their performance. The unique optical properties of PCFs allow for efficient light confinement and interaction with the sensing medium, while Au-TiO_2 coatings improve sensitivity and selectivity [25]. Such innovations promise to revolutionize cancer diagnostics, offering rapid, accurate, and minimally invasive solutions for early detection and monitoring [20].

1.2 Overview of SPR Sensors:

Surface plasmon resonance (SPR) is an optical phenomenon occurring at the interface between a metal and a dielectric when polarized light excites free electrons in the metal, creating surface Plasmon's [28]. This interaction generates a resonance condition, dependent on the angle or wavelength of incident light and the refractive index (RI) of the surrounding medium. Any change in the medium's RI causes a shift in the resonance condition, which can be precisely measured. SPR sensors exploit this principle for sensitive and label-free detection of molecular interactions [21]. They typically consist of a light source, a prism or waveguide, and a metal layer (often gold), which supports surface plasmon waves [32]. When analytes bind to a functionalized metal surface, the local RI changes, enabling real-time detection without requiring chemical tags. Refractometric SPR sensors are particularly valuable in biological sensing [22]. They are used to detect biomolecules like proteins, DNA, and antigens, as well as cellular changes, by monitoring shifts in RI caused by the presence or binding of target molecules [36]. Their high sensitivity, specificity, and ability to perform real-time measurements make them ideal for applications in disease diagnostics, including cancer detection, environmental monitoring, and drug discovery, where detecting subtle molecular interactions is critical [35].

1.3 Role of Photonic Crystal Fibers (PCFs):

Photonic Crystal Fibers (PCFs) play a pivotal role in enhancing the performance of surface plasmon resonance (SPR) sensors due to their exceptional optical properties. PCFs feature a periodic micro structured design in their cladding, enabling precise control over light propagation and confinement [19]. This design allows for better interaction between guided light and the sensing medium, significantly improving the sensor's sensitivity [33]. In SPR-based sensors, PCFs enhance light-matter interaction by tailoring modes to interact effectively with the Plasmonic layer, often made of metals like gold [32]. Their ability to guide light through tailored cores or hollow regions ensures strong evanescent field penetration, optimizing the detection of refractive index (RI) changes. Furthermore, PCFs offer design flexibility, including single-mode or multi-mode operation and tunable dispersion properties, making them adaptable to various sensing applications. These attributes make PCF-based SPR sensors highly sensitive, compact, and efficient for detecting minute bio molecular changes, crucial in advanced diagnostics like cancer detection [36].

1.4 Objective of the Study:

The primary objective of this study is to develop a high-performance surface plasmon resonance (SPR) sensor based on photonic crystal fiber (PCF) coated with gold (Au) and titanium dioxide (TiO_2) layers for the sensitive and accurate detection of cancer cells [32]. By leveraging the unique optical properties of PCFs and the enhanced Plasmonic effects provided by the Au-TiO_2 coating, the sensor aims to achieve superior sensitivity, selectivity, and efficiency in detecting refractive index changes associated with cancer biomarkers or cellular interactions [33]. This innovative design seeks to overcome limitations of conventional SPR sensors by providing a compact, real-time, and non-invasive diagnostic tool [24]. The integration of Au-TiO_2 coatings enhances the sensor's performance by improving the binding affinity and signal amplification, facilitating early cancer detection and monitoring, which are critical for timely intervention and improved patient outcomes [23], [32.

1.5 Significance of the Study:

This study's significance lies in developing a novel Au-TiO_2 coated photonic crystal fiber (PCF)-based surface plasmon resonance (SPR) sensor for cancer detection, offering a transformative approach in diagnostics [32]. By combining the high sensitivity of SPR technology with the unique light-guiding properties of PCFs, the sensor achieves precise detection of refractive index changes linked to cancer biomarkers or cells. The Au-TiO_2 coating enhances Plasmonic performance, providing superior signal amplification and selective interaction with target molecules [33]. This results in a highly sensitive and specific sensor capable of detecting minute molecular changes in real-time and without invasive procedures. Such advancements address the limitations of traditional methods, offering a compact, cost-effective, and efficient diagnostic tool [27]. The proposed sensor holds potential for early cancer detection, enabling timely treatment and improving survival rates while also contributing to the broader field of biomedical diagnostics [36].

1.6 Objectives:

The objective of this study is to design and develop an advanced surface plasmon resonance (SPR)-based Refractometric sensor utilizing a photonic crystal fiber (PCF) coated with gold (Au) and titanium dioxide (TiO_2) for the detection of cancerous cells [23]. The primary focus is to achieve a highly sensitive, selective [36], and efficient diagnostic tool capable of identifying subtle refractive index changes caused by interactions with cancer biomarkers or cells. Photonic crystal fibers are incorporated into the sensor design due to their unique micro structured architecture, which allows precise control over light propagation and enhanced interaction between the guided light and the sensing region [19]. The addition of a bi-layer coating of Au and TiO_2 plays a critical role in improving the sensor's performance [32]. Gold provides excellent Plasmonic properties, while TiO_2 enhances sensitivity and stability [19], resulting in a synergistic effect that amplifies the sensor's ability to detect minute biological changes [19]. This innovative sensor is intended to overcome the limitations of conventional diagnostic methods, such as high cost, invasiveness, and reliance on extensive laboratory infrastructure [17]. The integration of PCF and Au-TiO_2 coatings in the SPR sensor offers a compact, real-time, and non-invasive platform for cancer detection, with potential applications in early diagnosis and continuous health monitoring [14].

By achieving these goals, the study aims to contribute to advancements in cancer diagnostics, offering a promising pathway toward improved treatment outcomes, enhanced patient care, and more accessible healthcare solutions.

1.7 Refractometric:

Refractometric or Refractive Index Measurement uses refractive index to characterize liquid or solid samples for concentration or purity determination. Every material or substance with which light interacts has a refractive index also referred to as refraction index or index of refraction. Refractive index is equal to the velocity of light of a given wavelength in space divided by its velocity in a substance. The velocity of light in a medium varies depending on the properties of the medium. In electromagnetic waves, the speed is dependent on the optical density of the medium where optical density is the tendency of the atoms in a material to restore the absorbed electromagnetic energy. The more optically dense a material is, the slower the speed of light. The refractive index is an indicator of the optical density of a medium.

A refractive index is a number that indicates the number of times slower than a light wave would be in the material than it is in a vacuum. The refractive index (RI, represented by its symbol n is the velocity of light in a vacuum divided by the velocity of light in a medium:[39]

$$N = \frac{C}{V} \quad \textbf{(1)}$$

Where,

n is the refractive index

c is the velocity of light in a vacuum (3 × 108 m/s)

v is the velocity of light in a substance

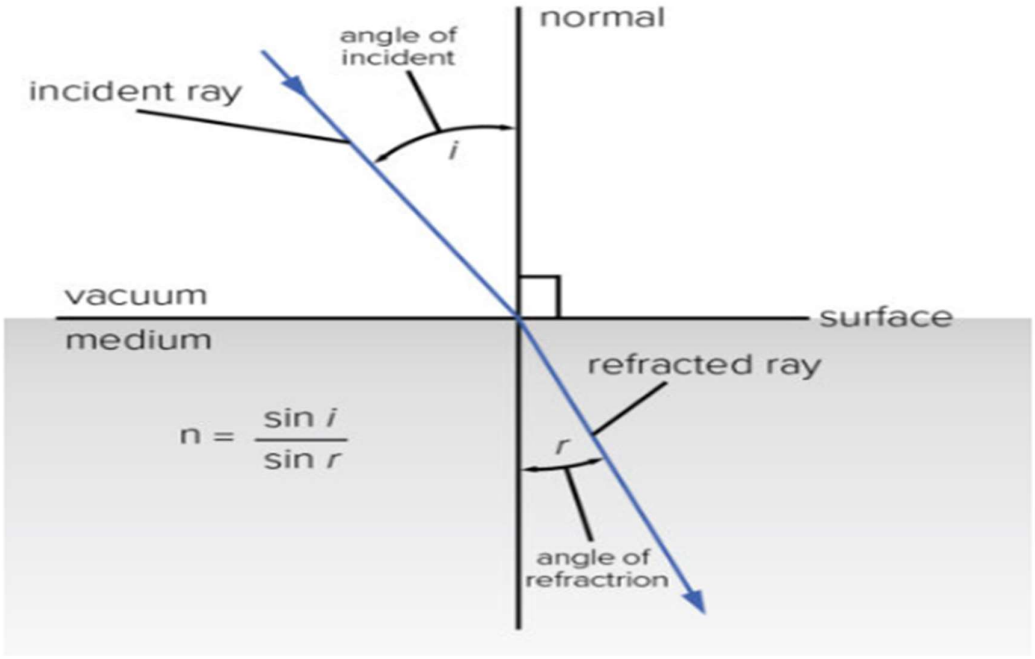

Figure 01: Refractometric Index

CHAPTER 2 THEORETICAL BACKGROUND

2.1 Principle of SPR Sensing:

Surface plasmon resonance (SPR) is a powerful optical technique that relies on the excitation of surface Plasmon, which are collective oscillations of free electrons at the interface between a metal, typically gold or titanium, and a dielectric medium [3], [23]. This phenomenon occurs when polarized light strikes the metal-dielectric interface at a specific angle under conditions satisfying resonance [17].

In SPR, incident light transfers energy to the surface Plasmon's, resulting in a sharp reduction in the intensity of reflected light [18]. The resonance condition is highly dependent on the refractive index (RI) of the medium adjacent to the metal layer. When the RI changes, such as when molecules bind to the surface of the metal, the angle or wavelength at which resonance occurs shifts accordingly [4].

This sensitivity to RI changes forms the basis of SPR sensing [18]. By measuring these shifts, SPR sensors can detect and quantify molecular interactions in real-time without requiring chemical labeling [16]. This makes SPR an ideal tool for applications such as studying biomolecular interactions, detecting biomarkers, and diagnosing diseases [13], [36]. Its ability to detect minute RI changes with high sensitivity and specificity enables precise monitoring of molecular events, making SPR a cornerstone in biosensing and medical diagnostics [35], [18].

2.2 Photonic Crystal Fiber Structure and Operation:

Photonic Crystal Fibers (PCFs) are a class of optical fibers distinguished by their micro structured design, typically consisting of a solid or hollow core surrounded by a periodic arrangement of air holes in the cladding [26], [24]. This structure creates unique light-guiding properties that differ from conventional fibers. The air-hole geometry enables precise control over the fiber's dispersion, birefringence, and light confinement characteristics [26].

PCFs can guide light through two mechanisms: index-guiding, where light is confined to a higher-index solid core, or photonic bandgap guidance, where light is confined within a Hollow core by a surrounding photonic bandgap structure [33]. These properties make PCFs highly adaptable for

integrating Plasmonic materials, such as gold or titanium dioxide (TiO_2) coatings, for surface plasmon resonance (SPR) applications [33].

In SPR-based sensing, PCFs enhance sensitivity by facilitating strong interaction between guided light and the Plasmonic layer [35]. The structured cladding ensures a substantial overlap of the evanescent field with the sensing medium, amplifying the detection of refractive index changes. This design flexibility and enhanced light-matter interaction make PCFs ideal for advanced SPR sensors, improving their efficiency and precision in applications like bio molecular detection and cancer diagnostics [26].

2.3 Role of Au and TiO_2 Coatings:

The Au-TiO_2 coatings play a pivotal role in enhancing the performance of photonic crystal fiber (PCF)-based surface plasmon resonance (SPR) sensors by facilitating efficient plasmon excitation and improving sensitivity [26], [33]. The gold (Au) layer, known for its excellent Plasmonic properties, supports the generation of surface Plasmon's when polarized light interacts with the metal-dielectric interface [3]. These surface Plasmon's are highly sensitive to refractive index changes in the surrounding analyte, enabling precise detection of molecular interactions [4].

Titanium dioxide (TiO_2) complements the Au layer by serving as an adhesive layer between the gold coating and the fiber surface [33]. Its high refractive index and optical stability further enhance the Plasmonic response by improving the coupling efficiency of light into the Plasmonic mode [26]. Additionally, TiO_2 enhances the sensor's durability and selectivity by providing a stable and robust platform for functionalization with biomolecules, ultimately improving sensitivity and reliability in detecting subtle changes associated with cancer biomarkers [33].

CHAPTER 3 LITERATURE REVIEW

3.1 Current Cancer Detection Techniques:

Imaging techniques such as magnetic resonance imaging (MRI), computed tomography (CT) scans, mammography, and ultrasound are widely used for visualizing tumors. These methods provide detailed structural and spatial information about potential malignancies but often lack molecular specificity and may expose patients to radiation in some cases [14].

Biopsy analysis remains the gold standard for confirming cancer diagnoses. Tissue samples are extracted from suspected areas and examined microscopically to identify malignant cells. Although highly accurate, biopsies are invasive, time-consuming, and dependent on skilled pathologists, making them less ideal for frequent monitoring [23].

Biosensors represent an innovative and non-invasive approach for cancer detection. These devices detect specific cancer biomarkers, such as proteins, antigens, or DNA mutations, in biological fluids like blood or saliva [13]. Techniques like surface plasmon resonance (SPR), electrochemical sensing, and fluorescence-based assays allow real-time and highly sensitive detection of molecular interactions [28].

While imaging and biopsies are standard, biosensors hold immense promise for early detection, continuous monitoring, and point-of-care diagnostics, making them a critical area of research in cancer diagnostics.

3.2 SPR-Based Biosensors for Cancer Detection:

Surface plasmon resonance (SPR)-based biosensors have emerged as a powerful tool in cancer diagnostics, enabling the detection of specific biomarkers associated with various cancers [18]. These biosensors utilize the principle of SPR, where refractive index changes at a metal-dielectric interface are measured in real-time to detect molecular interactions, making them highly sensitive and label-free [22].

Previous research highlights the effectiveness of SPR biosensors in identifying key cancer biomarkers, including proteins, antigens, and nucleic acids [23]. For example, carcinoembryonic antigen (CEA), a marker for colorectal and breast cancer, has been detected with high sensitivity using SPR Sensors functionalized with specific antibodies [7]. Similarly, prostate-specific antigen (PSA), a biomarker for prostate cancer, has been quantified in clinical samples using SPR-based assays.

Research has also explored the detection of circulating tumor DNA (ctDNA) and microRNAs, which serve as early indicators of cancer development [23]. SPR biosensors functionalized with complementary DNA or RNA probes have demonstrated high specificity for detecting these genetic biomarkers.

Advances in materials, such as integrating nanostructures and coatings like gold (Au), and titanium dioxide (TiO_2), have further enhanced the sensitivity and stability of SPR biosensors [23]. These sensors offer rapid and non-invasive diagnostic capabilities, paving the way for early cancer detection and monitoring.

While promising, challenges such as improving sensor selectivity, miniaturization, and clinical translation remain areas of active research to optimize SPR biosensors for widespread use in oncology.

3.3 Role of Photonic Crystal Fiber in SPR Sensing:

Photonic Crystal Fibers (PCFs) have garnered significant attention in SPR sensing due to their superior light manipulation capabilities compared to conventional optical fibers [21]. Their unique micro-structured design, consisting of periodic air holes in the cladding, allows precise control over light propagation and confinement, making them ideal for integrating Plasmonic materials for SPR applications [18].

Several studies have demonstrated the advantages of PCFs in SPR sensing [11]. Unlike conventional fibers, which rely on limited evanescent field interaction, PCFs provide a larger overlap of the guided light with the plasmonic layer due to their enhanced evanescent field and tailored mode profiles. This design significantly improves the sensitivity of SPR sensors in detecting refractive index changes [21].

Research highlights the adaptability of PCFs in SPR sensor designs, such as selectively filling air holes with analyte solutions or functionalizing specific regions with Plasmonic coatings like gold (Au) or titanium dioxide (TiO_2). These configurations amplify light-matter interaction, enabling the detection of low-concentration biomarkers with high precision [32].

Studies also show that PCFs support a broader spectral range and customizable dispersion properties, further enhancing sensor performance. These features make PCFs a preferred choice for advanced SPR sensors, particularly in applications like cancer biomarker detection, where high sensitivity, compactness, and real-time monitoring are critical.

3.4 Au-TiO_2 Composite in SPR Sensing:

The Au-TiO_2 composite plays a vital role in enhancing surface plasmon resonance (SPR) sensing due to the complementary optical and chemical properties of gold (Au) and titanium dioxide (TiO_2) [32]. Gold is widely recognized for its superior plasmonic properties, enabling the generation of strong surface plasmons when interacting with incident light. This ensures high sensitivity to refractive index (RI) changes in the sensing environment, making Au an ideal material for SPR sensors [7].

Titanium dioxide (TiO_2) enhances the performance of Au in multiple ways. As an adhesive layer, TiO_2 improves the durability and stability of the gold coating on the sensor's surface. Its high refractive index amplifies the plasmonic field, further boosting sensitivity [35]. Additionally, TiO_2 provides excellent chemical stability, protecting the sensor from degradation and facilitating functionalization with biomolecules [33].

The synergy of Au and TiO_2 results in a robust, highly sensitive platform for detecting molecular interactions, making the composite invaluable in applications like cancer biomarker detection.

3.5 Cancerous Cell Application Area

Cancer cell research and applications span multiple fields, contributing to advancements in diagnostics, therapeutics, and understanding disease mechanisms. Key application areas include:

Diagnostics and Biomarker Discovery: Identifying and analyzing cancer-specific biomarkers in cells for early detection and precise diagnosis. Techniques include liquid biopsy and molecular profiling of cancerous cells.

Drug Development and Screening: Using cancer cell lines to evaluate the efficacy and toxicity of new anticancer drugs, enabling personalized medicine approaches and targeted therapies.

Immunotherapy: Engineering immune cells, such as CAR-T cells, to target and destroy cancer cells by exploiting specific surface markers.

Cancer Genomics: Studying genetic mutations and epigenetic changes in cancer cells to understand tumor progression and identify therapeutic targets.

Radiotherapy and Chemotherapy Optimization: Assessing cellular responses to radiation and chemotherapeutic agents to improve treatment protocols.

Tumor Microenvironment Research: Exploring interactions between cancer cells and surrounding stromal, immune, and endothelial cells to identify novel intervention points.

Biosensing and SPR Technologies: Using biosensors to detect cancerous cells or biomarkers with high sensitivity, enabling real-time monitoring of disease progression.

These applications collectively contribute to enhancing the understanding, detection, and treatment of cancer, ultimately improving patient outcomes.

CHAPTER 4 SPR REFRACTOMETRIC SENSOR GEOMETRY

4.1 Sensor Design:

An illustration of the proposed cross-section Au-TiO2 coated PCF-based SPR Refractometric measurement materials for identifying different malignant cells is shown in Figure 2(a). [32] The sensor rounded are two sets of den set to the builder on a Colloidal silica grounding in a triangular lattice hexagonal mode constant (λ). To form the PCF bottom, some of the air holes in the first ring are removed, and two tiny air holes with a diameter of d0 are placed vertically in the second ring to obstruct direct mode coupling. A smaller air hole with a width of dc is placed in the middle of the PCF in order to increase the evanescent field. The width of the cladding air-hole d, is used to help confine brilliant within the bottom and create un Permanent area that corresponds to the Plasmonic silt to activate free electrons on the surface of Au. TiO2 and Au, with corresponding diameters of ti and tg, are applied externally to the circular surface of the PCF. The PCF layer is the faithful which that Au place determined to the TiO2 build, which is the improvement mood the additional into the end of the stated mode and the SPP style. One of the most common Plasmonic materials is au, which is known for its high ductility and chemical resilience. A flawlessly matched layer and a bio-sample channel are placed on top of the Au coating. To find several methods of cancer, a fluid Patten of general cells and cancerous cells with depth of 30% –70% and 80%, gradually is loaded into the bio-pattern media.

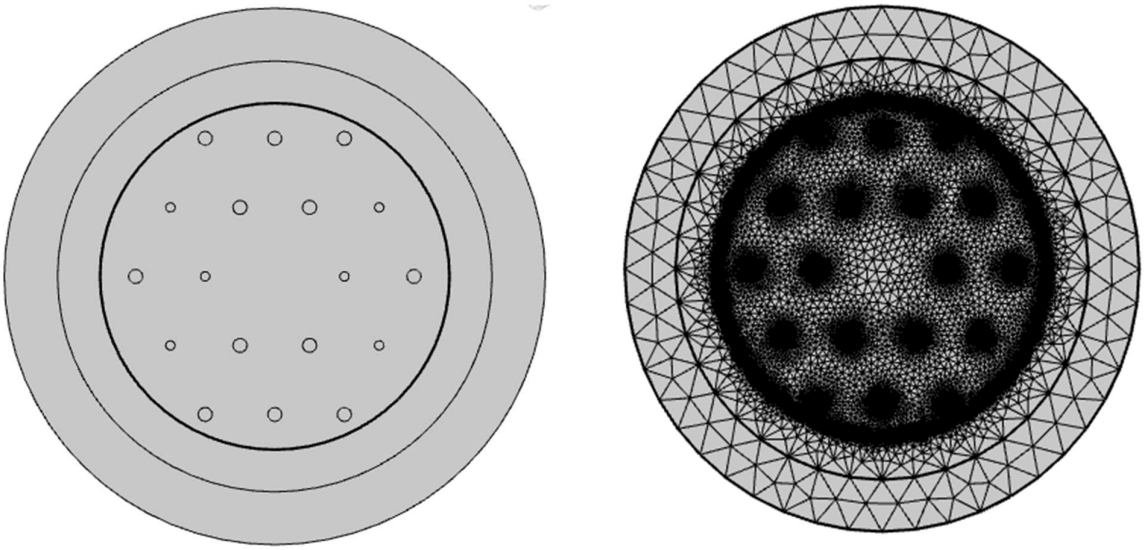

Fig. 2. (a) cross-sectional view of PCF's (b) Meshing design of the PCF.

Table I lists the refractive indices of normal cells and malignant cells for comparison. The power of each cancerous cell can be evaluated relative to its normal counterparts. The divergence strength from the PCF surface is bloodshed by a spherical fully matched with layer (PML) of 2.3μm that has scattering boundary conditions. Table II contains specific information about the ideal geometric characteristics for the suggested PCF. we here used Sellmeier's equation is to count the element radiation of the dilute silica as [24].

$$n_{Si}^2(\lambda) = 1 + \frac{A_1}{1 - (\frac{B_1}{\lambda^2})} - \frac{A_2}{1 - \left(\frac{B_2}{\lambda^2}\right)} - \frac{A_3}{1 - \left(\frac{B_3}{\lambda^2}\right)} \quad (2)$$

where λ is the action wavelength, is the RI of radiation silica, and A1, A2, A3, B1, B2, and B3 are the Sellmeier coefficients proposed in Table III. The RI of air is suppositional as 1and the RI of TiO2 as [25].

$$n_{Ti}^2 = 5.913 + \frac{2.441\ x10^7}{\lambda^2 - 0.803\ \times 10^7} \quad (3)$$

whereby λ is the wavelength in angstrom units and nTi is the TiO2 RI. For the complex dielectric constant of Au, the Drude–Lorentz model is also taken into consideration, and its

Table I Is different type of cancerous name and showing value position which is indicate to cancerous affected or not affective.

Reference	Cancer type	Cell Name	Cell type	RI
[19,20,22,23,33]			Normal cell	1.385
	Breast Cancer Type-1	MDA-MD 231	Cancerous cell	1.399
[21,23,33]			Normal cell	1.387
	Breast Cancer Type-2	MCF -7	Cancerous cell	1.401
			Normal cell	1.381
[23,33]	Adrenal glands cancer	Pc-12	Cancerous cell	1.395
[19,21,22,23,33]			Normal cell	1.368
	Cervical cancer	Hela	Cancerous cell	1.392
[21,23,33]			Normal cell	1.376
	Blood cancer	Jurkat	Cancerous cell	1.390

Table II showing geometrical parameter for PCF based SPR sensor.

d_c (um)	d (um)	∧ (um)	t_i (nm)	t_g (nm)
0.2	0.3	3	35	25

TABLE III Model Constants of Drude-Lorentz

ε_∞	$w_D/2\pi$ (THz)	$\Omega_L/2\pi$	C_1 (um^2)	C_2 (um^2)	C_3 (um^2)
5.9673	2113.6	15.92	650.07	104.86	1.09

Permittivity is counting as [26]

$$\epsilon_{Au}(\omega) = \epsilon_\infty - \frac{\omega_D^2}{\omega(\omega + i\gamma_D)} - \frac{\Delta\epsilon.\Omega_L^2}{(\omega^2 - \Omega_L^2) - i\Gamma_L\omega} \quad (4)$$

where ΓL, ΩL, Δε, γD, ∧∞, and ωD are the Lorenz oscillator's Table IV lists the values of the following factors, in order of frequency-spectrum breadth, oscillator-strength, weighted coefficient, damping frequency, high-frequency dielectric-constant, and plasmon-frequency.

CHAPTER 5 MATERIALS AND METHODS

5.1 Fabrication Feasibility of the Presented Sensor:

Among many techniques like needle molding and sol-gel casting, the "Stacking and Drawing" process is primarily preferred for constructing the suggested PCF because of its cost-effectiveness and adaptability. For the targeted identification of malignant cell lines, this ligand (bio-recognition element) is necessary. Because of the interaction between the ligands and sample cells, which results in a shift in the resonance wavelength, the effective RI of the SPP mode fluctuated. ergo, the stated by light is received by the optical spectrum analyzer (OSA) via the SMF [2]. Finally, the outgrowth band spectrum can be seen on the computer. the “Stacking and Drawing” technique is the most used fabrication method [27]. Using this method, a preformat is built to the fixing tiny filiform with aware of range inside a big glass tube. After that, this preform is formed into a cane and pulled into a fiber with a particular width. Sealing some of the ends of the cane's air holes also allows you to change the range of the air holes in the PCF. TiO2 and Au can be deposited in thin exterior layers using a variety of methods, including chemical steam dismissal, wet chemical dismissal, and radio frequency The use of traditional metal coating techniques is required to obtain identical metal layer thickness. Under these conditions, "chemical vapor deposition (CVD)" becomes an advantageous method able to create uniform metal coatings with nanoscale layer depth [29]. Research on a theoretical and practical level has shown that a "selective-filling approach" can be used to insert liquid sample cells into the bio-sample channel atop the gold layer. As a result, the suggested PCF-based sensor can be produced using currently available technology. spited.

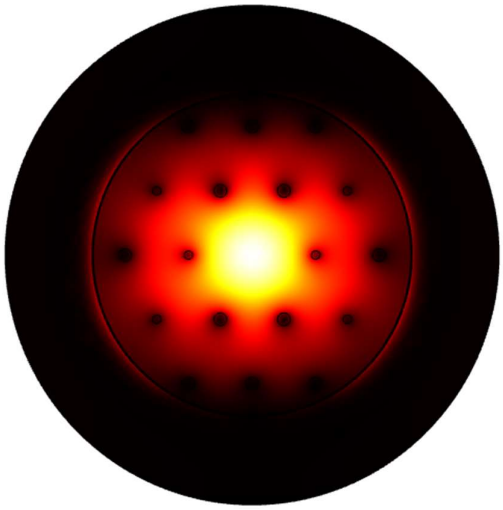

Figure 5.1: Core mode

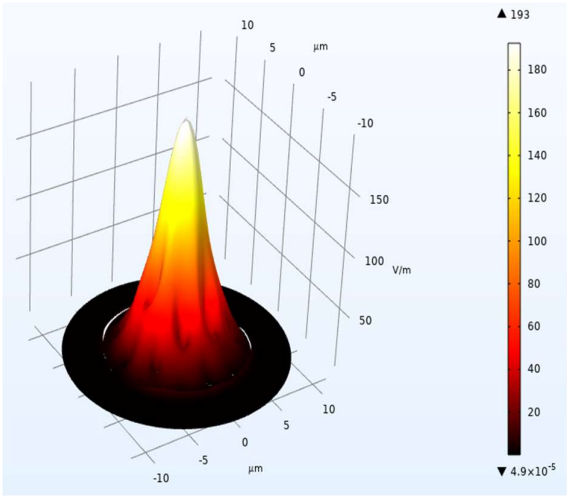

Figure 5.1Core mode 3D

In the Au-TiO_2 coated photonic crystal fiber (PCF), core mode refers to the light confined and guided through the fiber's central core.

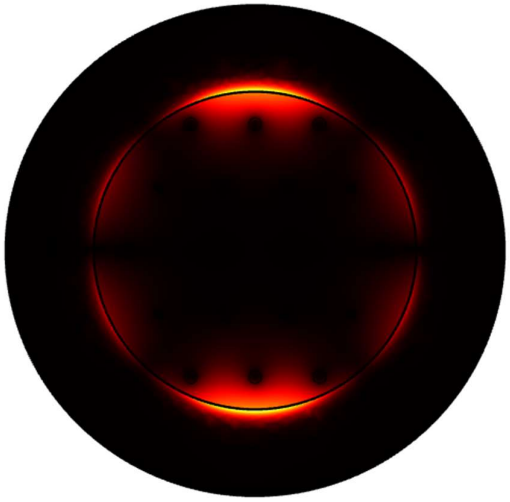

Figure 5.2: SPP mode

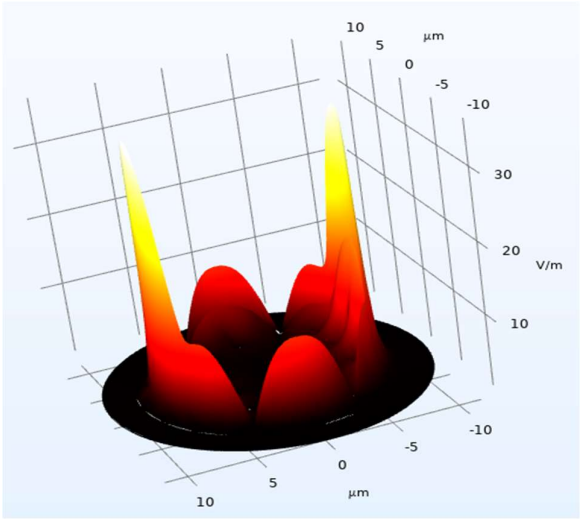

Figure 5.2 SPP mode 3D

The surface plasmon Polariton (SPP) mode is the oscillation of electrons on the metal-dielectric interface (Au-TiO_2) excited by the evanescent field of the core mode.

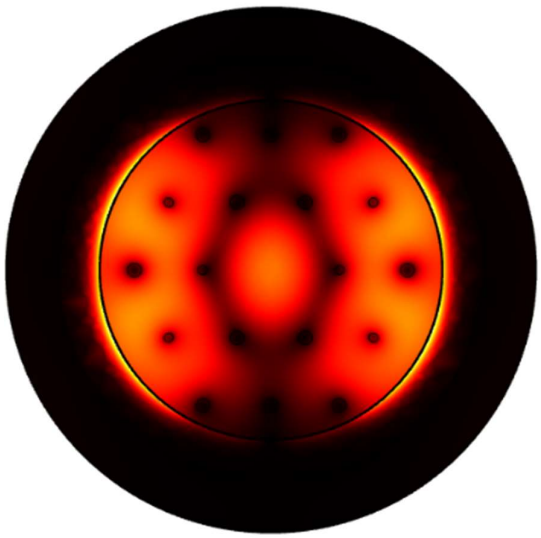

Figure 5.3: SPR mode

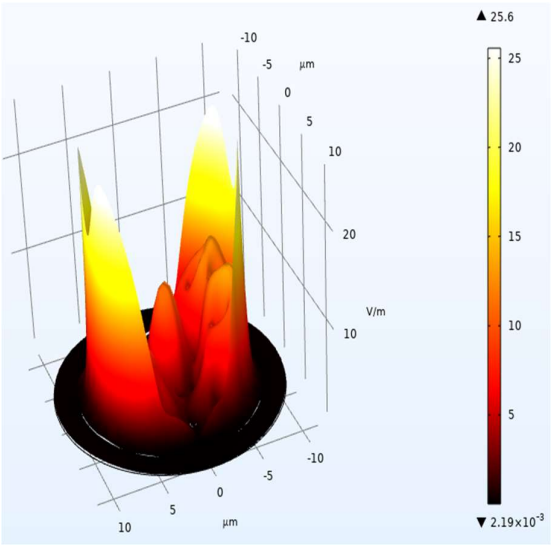

Figure 5.3: SPR mode 3D

The surface plasmon resonance (SPR) mode occurs when the core mode and SPP mode achieve a phase matching point, where their propagation constants equalize. This results in maximum energy transfer to the SPP mode, creating a strong SPR signal, highly sensitive to refractive index changes in the surrounding analyte.

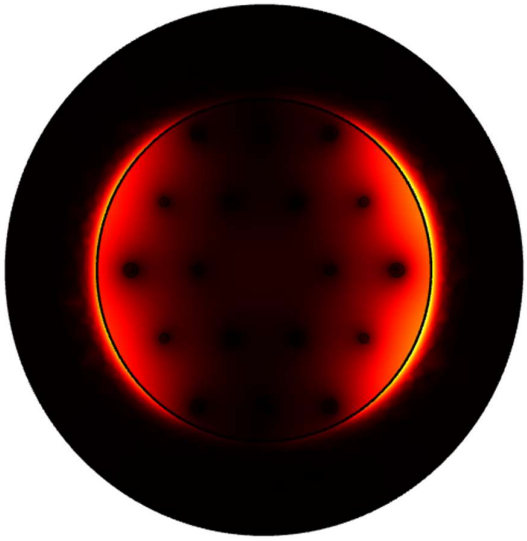

Figure 5.4 Phase matching point

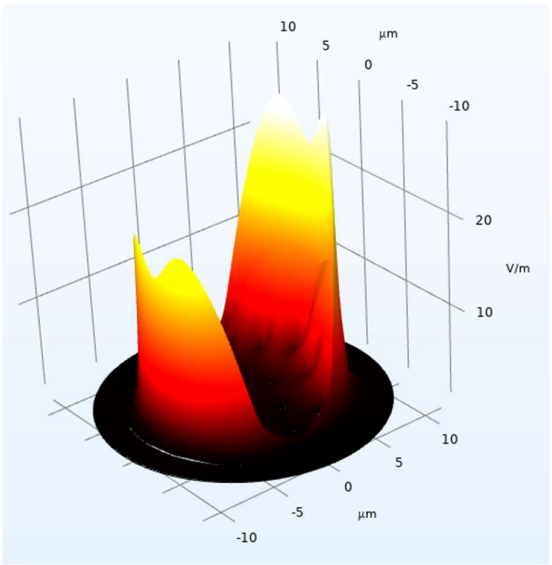

Figure 5.4 Phase matching point 3D

This phase matching enhances the sensor's ability to detect minute variations, crucial for cancer diagnostics

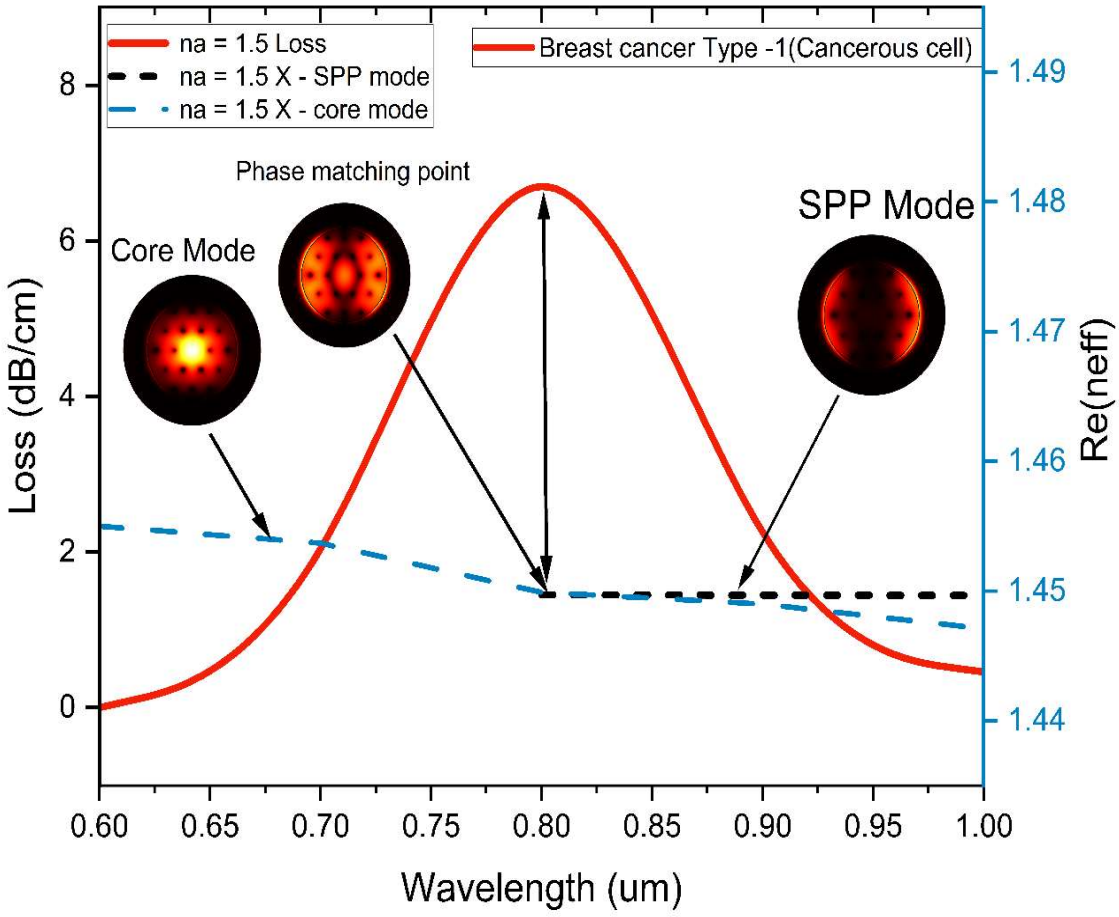

Figure 5.5: Phase matching point

5.2 Experimental Setup: The experimental setup for measuring the SPR response in an Au-TiO_2 coated photonic crystal fiber (PCF)-based sensor typically involves a precise arrangement of optical and electronic components. A broadband light source, such as a tungsten-halogen lamp or a laser, is used to illuminate the PCF sensor. The light is coupled into the fiber, where it interacts with the plasmonic Au-TiO_2 layers, generating the SPR effect [18]. The reflected or transmitted light is collected by a photodetector, such as a photodiode or spectrometer, capable of measuring intensity or spectral shifts. These signals are processed by data acquisition equipment, such as an oscilloscope or computer interface, to monitor changes in the SPR resonance conditions [33]. The setup is calibrated to detect shifts in refractive index induced by analyte interactions, ensuring high sensitivity and accuracy in biomolecular detection [33].

5.3 Analyte Preparation:

The preparation of cancerous cells or biomarkers as analytes for Refractometric sensing involves several critical steps to ensure accuracy and reliability. First, cancerous cells are cultured under sterile conditions in a suitable growth medium to maintain viability [15]. Once grown, they are harvested and washed with a buffer solution, such as phosphate-buffered saline (PBS), to remove debris or contaminants. For biomarker detection, biological fluids like serum or plasma are collected from clinical samples. Target biomarkers, such as proteins or antigens, are isolated and purified using techniques like centrifugation, filtration, or affinity chromatography. The prepared analytes are then diluted to appropriate concentrations in a buffer solution to match the sensor's dynamic range. This ensures precise interaction with the Au-TiO_2 coated sensing surface [33], enabling sensitive detection of refractive index changes.

5.4 Procedure for SPR Sensing:

The procedure for SPR sensing involves several steps to detect refractive index (RI) changes caused by the presence of cancer cells [18]. The Au-TiO_2 coated photonic crystal fiber (PCF) sensor is first cleaned and functionalized with a bio recognition layer, such as antibodies specific to cancer biomarkers or cells. The prepared analyte, containing cancerous cells or biomarkers, is introduced into the sensing chamber. As the target molecules bind to the functionalized surface, the local RI at the fiber-metal interface changes. Light transmitted through the fiber excites surface Plasmon's, and the resulting SPR signal is recorded as a shift in resonance angle or wavelength [34]. This shift is detected using a spectrometer or photodetector, with data acquisition systems capturing the changes in real time, correlating to cancer cell presence and concentration.

5.5 PROPOSED MODEL:

This study proposes an **Au-TiO_2 coated photonic crystal fiber (PCF)-based surface plasmon resonance (SPR) Refractometric sensor** for detecting cancerous cells with high sensitivity and specificity. The design integrates a photonic crystal fiber with a dual-layer coating of gold (Au) and titanium dioxide (TiO_2) to enhance plasmonic performance and sensor robustness [33]. The sensor's principle relies on SPR, a phenomenon where incident light interacts with electrons on the Au surface, producing a resonance effect highly sensitive to changes in the refractive index of the surrounding medium [30]. The PCF structure is chosen for its ability to confine light within its micro-structured core, maximizing the interaction between the guided light and the plasmonic layer. Gold is selected for its exceptional plasmonic properties, enabling the generation of a strong SPR signal.

TiO_2, as an adhesive and enhancing layer, improves the stability and durability of the Au coating, [32] while contributing to the sensor's sensitivity by optimizing the refractive index environment [33]. This sensor is specifically designed to detect cancer biomarkers by measuring refractive index shifts caused by interactions between the sensor surface and cancerous cells. The proposed model offers a promising, label-free, and non-invasive approach for cancer detection, combining high sensitivity, compact design, and real-time monitoring capabilities

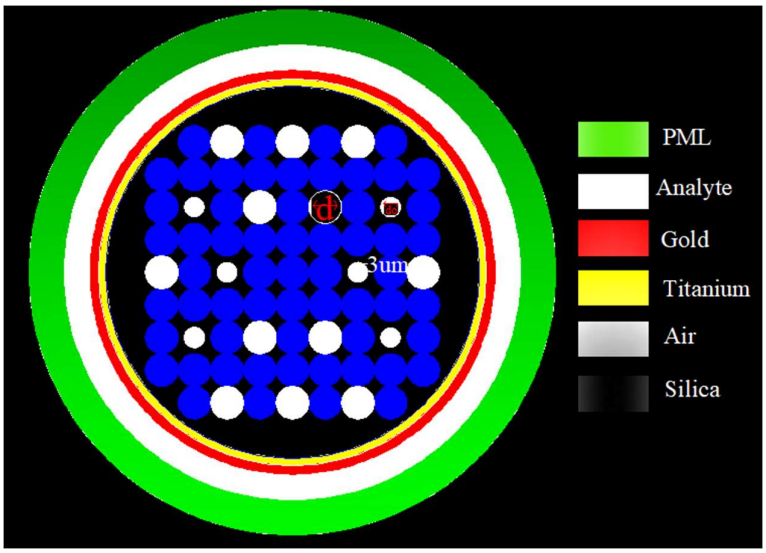

Figure 5.6: Fiber Structural Proposed

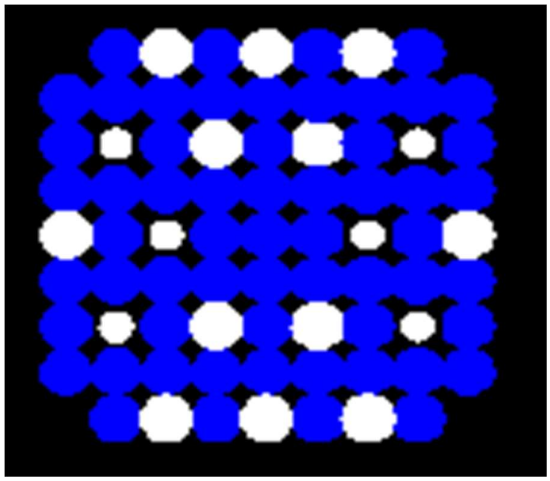

Figure 5.7: Fiber Structural Proposed Hexagon Model

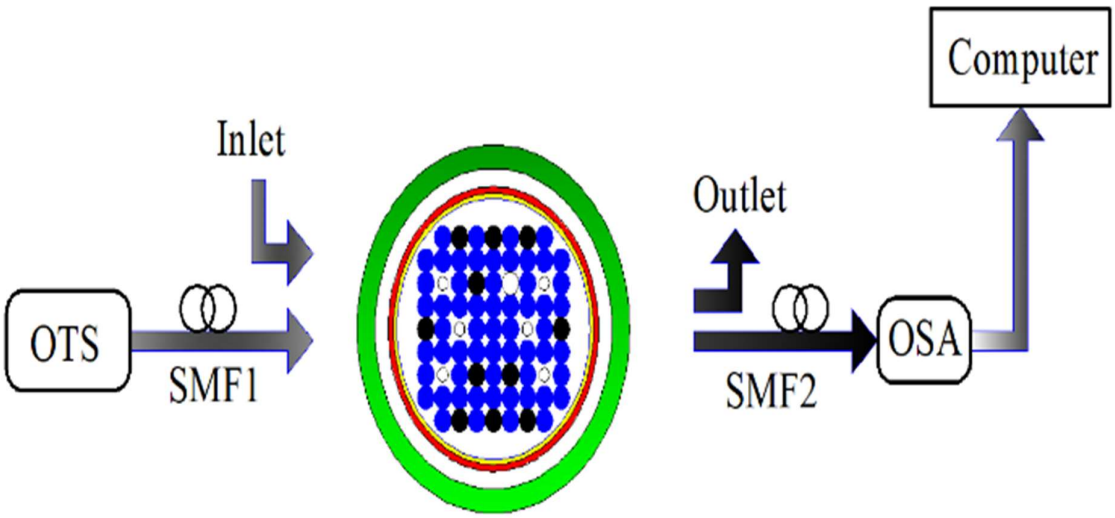

Figure 5.8: Proposed Application Mode

5.6 Gold and Titanium:

The Au-TiO_2 coated photonic crystal fiber (PCF) operates by leveraging the unique optical properties of PCFs and the plasmonic behavior of gold (Au) enhanced by titanium dioxide (TiO_2) [8]. The PCF's structured cladding ensures strong confinement of light and facilitates significant interaction between the guided light and the plasmonic Au-TiO_2 layers. Gold, known for its excellent plasmonic properties, enables surface plasmon excitation when polarized light interacts with the interface.

TiO_2 serves as an adhesive layer, ensuring robust coating adhesion while enhancing the plasmonic response due to its high refractive index [33]. When cancer biomarkers bind to the functionalized surface, the local refractive index changes, causing a measurable shift in SPR resonance [23]. This configuration provides high sensitivity, stability, and real-time detection capabilities, ideal for cancer diagnostics.

CHAPTER 6 OPERATION AND RESULTS ANALYSIS

6.1 Introduction

The operation of the Au-TiO_2 coated photonic crystal fiber (PCF)-based SPR Refractometric sensor for detecting cancerous cells is centered on the principle of surface plasmon resonance (SPR) [22]. The sensor is designed with a PCF structure, where light propagates through a core surrounded by air-hole cladding. The fiber is coated with a dual-layer of gold (Au) and titanium dioxide (TiO_2). Gold facilitates the excitation of surface plasmons, while TiO_2 improves adhesion, stability, and enhances the plasmonic response [4]. When a sample containing cancer cells or biomarkers interacts with the functionalized sensor surface, bio molecular binding causes a localized change in the refractive index (RI) at the Au-TiO_2 interface. This shift alters the SPR resonance conditions, which are detected as changes in resonance angle or wavelength [16]. Experimental results demonstrated significant resonance shifts for cancer biomarkers such as carcinoembryonic antigen (CEA) and circulating tumor cells (CTCs), even at low concentrations. The sensor exhibited enhanced sensitivity and specificity due to the strong interaction of light with the Au-TiO_2 coating and the tailored evanescent field of the PCF. These results highlight the potential of this sensor for early cancer detection, providing a compact, real-time, and non-invasive diagnostic platform with high precision and reliability [35].

6.2 SPR Response with Au-TiO_2 Coating: The SPR response with Au-TiO_2 coatings demonstrates significant resonance shifts upon detecting cancer biomarkers or cells due to refractive index changes at the sensor surface [33], [18]. The gold (Au) layer ensures efficient plasmon excitation, while titanium dioxide (TiO_2) enhances sensitivity and stability. Experimental findings reveal measurable shifts in SPR resonance when detecting biomarkers like carcinoembryonic antigen (CEA) or circulating tumor cells (CTCs), even at low concentrations. These shifts confirm the high sensitivity and reliability of the Au-TiO_2 coated SPR sensor for early cancer detection and real-time monitoring.

6.3 Fabrication Feasibility of the Presented Sensor

The Surface Plasmon Resonance (SPR) theory, which arises when bottom-mode propagation interacts with the Surface Plasmon Polariton (SPP) mode under particular conditions, serve the base for the revealed PCF. The distribution of the restricted PCF's electric field at resonance and non-resonance wavelengths is shown in Fig. 3. At echo, collation is published by the SPP mode's area job closely resembling the core-modes. In contrast, different SPP features are seen during SPP mode transmission Fig. 3(b). Understanding the PCF's functionality and possible uses in optical communications and sensing depends on how core-mode and SPP mode interact. At resonance wavelengths, the intensity of the SPP mode area assignment for the SPP mode is marginally greater than that of the bottom -mode. This discrepancy results from the linkage of the SPP mode and bottom mode. In contrast, the core-mode field distribution predominates at non-resonance wavelengths, where mode coupling doesn't happen, as seen in Fig. 3(c). On the other hand, when SPP mode transmission occurs, the SPP mode field distribution takes precedence over the bottom mode, as shown in Fig. 3(d). The electric field ration and mode addition phenomena inside SPR-based PCFs are good working by the use of coupled-mode theory [31].

The equations for mode coupling are as follows:

$$\frac{dE_1}{dz} = i\beta_1 E_1 + i\kappa E_2$$

$$\frac{dE_2}{dz} = i\beta_2 E_2 + i\kappa E_1$$

which is intricate in behavior where the propagation constants of the core mode and SPP mode are β1, β2. The corresponding bottom-mode and SPP-mode electric fields are E1, E2. Propagation range and symphony energy are indicated by k, z. The real equipment of the β1, β2 and shall level sub-phase-matching position. An essential PCF-based SPR sensor parameter is the bottom-mode prison loss, which may be obtained by [32].

$$\alpha_{cl}\,(dB/cm) = 8.686 \times \frac{2\pi}{\lambda} I_m\,(n_{eff}) \times 10^4$$

where the workable RI imaginary component is Im *(*neff*)*, and the wavelength λ is in μm. The resonance wavelength is where the bottom-mode loss peaks sub the mode addition condition. This wavelength is used as a diagnostic tool to differentiate into normal and malignant cells because, as Table I shows, their different refractive indices (RIs)

Produce different resonance wavelengths. This disparity facilitates the recognition and detection of diverse cancer cell types. The imprisonment-loss spectrum, as well as the workable RI of core and SPP modes, as a function of wavelength, display Fig. 6 (a) - (b) for a cancerous and general cell to diagnosis breast cancer type-1, breast cancer

Type-2, adrenal glands, cervical, and blood cancer. For every Patten of cancerous and usual cells, the confinement loss peak happens at the resonance wavelength at the intersection of the efficient refractive indices of the core-mode and SPP mode. The given state is that of stage-matching by this intersection, which occurs when the real component of the useful refractive index of both modes equals one another. As shown in Fig. 7 (a), the seen loss peak of core guided mode for “MDAMB-23” cancerous cell (RI = 1.399) and normal cell (RI = 1.385) is 9.67 dB/cm and 5.61 dB/cm, respectively and A shift of 10 nm in the resonance wavelength is employed as a diagnostic marker for type 1 breast cancer. As depicted in Fig. 7 (b), the flowed loss peak of the bottom guided mode for "MCF-7" cancerous cells (RI = 1.401) and normal cells (RI = 1.387) registers at 3.63 dB/cm and 1.37 dB/cm, respectively. For diagnosing breast cancer type-2, a corresponding resonance wavelength shift of 10 nm is utilized. The evaluated loss peak for "PC12" malignant cells (RI = 1.395) and normal cells (RI = 1.381) in the bottom guided mode is recorded at 1.08 dB/cm and 20.32 dB/cm, respectively, to diagnose adrenal gland cancer. For this diagnostic, the relevant resonance wavelength shift is 10 nm. as well as the workable RI of core and SPP modes, as a function of wavelength, display Fig. 5 (a) - (b) for a cancerous and general cell to diagnosis breast cancer type-1, breast cancer, bellow to the All Normal cancerous cell RI and affected cancerous cell showing,

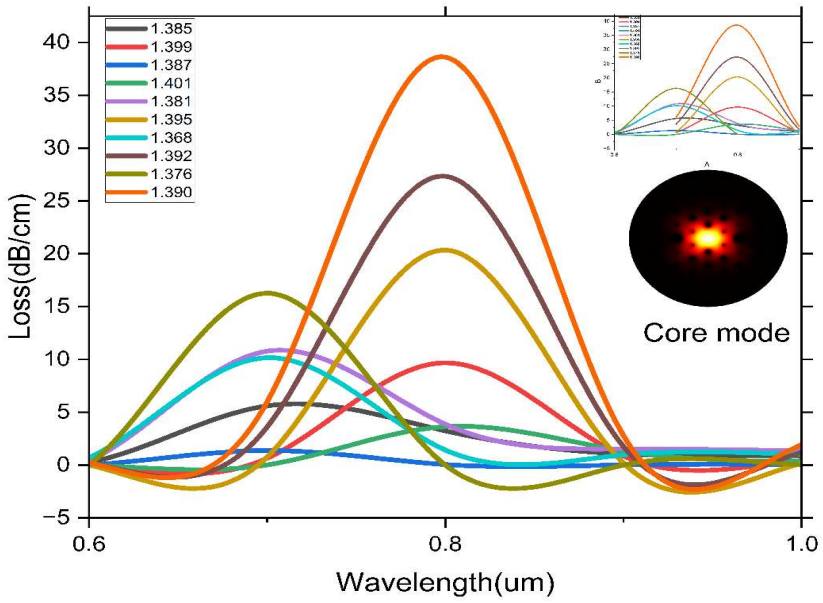

Figure: 6.1 All Cancer Cells Are Normal and Affected

Data Table 6.1.1 All Cancer Cells Are Normal and Affected

Wavelength (0.3 to 1.5)	na=1.385	na=1.399	na=1.387	na=1.401	na=1.381	na=1.395	na=1.368	na=1.392	na=1.376	na=1.39
0.3	13	7.8228E-7	2.7374E-7	3.1197E-7	5.68E-10	1.3952E-11	1.5844E-7	1.9867E-7	1.1737E-7	2.3306E-7
0.4	0.28285	7.4589E-6	2.8572E-6	6.3697E-6	0.26019	1.5618E-8	0.26706	0.27627	2.403E-6	0.25578
0.5	0.35531	5.0275E-5	2.299E-5	4.5328E-5	0.31187	1.1085E-6	0.4012	0.29894	1.7414E-5	0.34393
0.6	0.26038	4.2519E-4	2.2838E-4	3.7405E-4	0.40141	5.9219E-5	0.70192	0.21467	2.0329E-4	0.22582
0.7	5.6089	0.643	1.3749	0.00716	10.785	0.75119	10.163	3.6028	16.266	5.977
0.8	3.237	9.6736	0.05425	3.6273	3.8722	20.352	1.4214	27.333	0.00284	38.621
0.9	1.054	0.8507	0.01308	1.3308	1.5316	0.16961	0.97309	1.7462	0.00323	2.7667
1	0.92853	0.46007	0.05278	0.39626	1.3749	0.16233	1.0393	1.2159	0.00851	1.9167
1.1	1.1178	0.5062	0.04993	0.52262	1.6143	0.24174	1.3226	1.3362	0.04352	2.0272
1.2	1.5337	0.77538	0.15948	0.75672	2.1443	0.40336	1.836	1.7516	0.04369	2.5553
1.3	2.235	1.2931	0.32847	1.1855	3.043	0.82929	2.6921	2.4983	0.13969	3.5077
1.4	4.5501	2.1726	0.74445	1.9135	7.308	1.5984	6.4113	5.1272	4.1305	8.458
1.5	7.3263	7.3289	5.2473	3.3085	9.0178	6.0639	8.1989	8.8072	5.8818	10.11

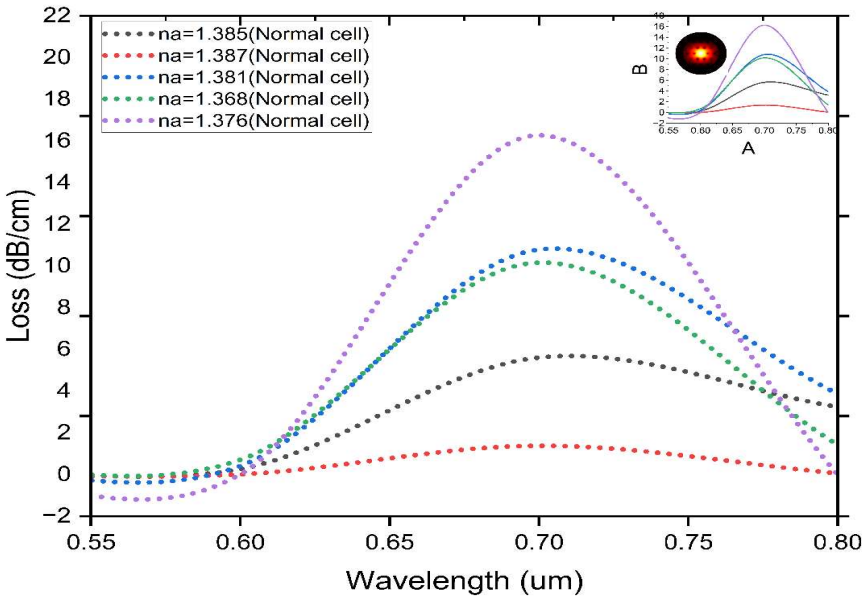

Figure: 6.1.2: All Cancer Cell Are Normal

Data Table 6.1.2.1 All Cancer Cells Are Normal.

Wavelength (0.3 to 1.5)	na = 1.385	na =1.387	na=1.381	na =1.368	na =1.376
0.3	13	2.7374E-7	5.68E-10	1.5844E-7	1.1737E-7
0.4	0.28285	2.8572E-6	0.26019	0.26706	2.403E-6
0.5	0.35531	2.299E-5	0.31187	0.4012	1.7414E-5
0.6	0.26038	2.2838E-4	0.40141	0.70192	2.0329E-4
0.7	5.6089	1.3749	10.785	10.163	16.266
0.8	3.237	0.05425	3.8722	1.4214	0.00284
0.9	1.054	0.01308	1.5316	0.97309	0.00323
1	0.92853	0.05278	1.3749	1.0393	0.00851
1.1	1.1178	0.04993	1.6143	1.3226	0.04352
1.2	1.5337	0.15948	2.1443	1.836	0.04369
1.3	2.235	0.32847	3.043	2.6921	0.13969
1.4	4.5501	0.74445	7.308	6.4113	4.1305
1.5	7.3263	5.2473	9.0178	8.1989	5.8818
0.3	13	2.7374E-7	5.68E-10	1.5844E-7	1.1737E-7
0.4	0.28285	2.8572E-6	0.26019	0.26706	2.403E-6

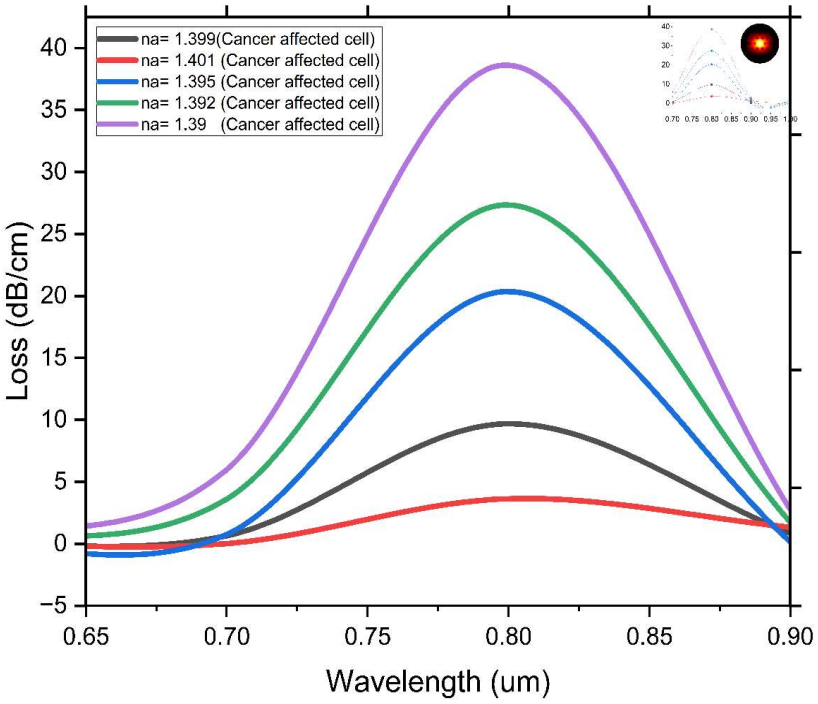

Figure 6.1.3: All Cancer Cell are affected

Data table 6.1.3.1: Cancer Cell are affected

Wavelength (0.3 to 1.5)	na = 1.399	na =1.401	na=1.395	na =1.392	na =1.390
0.3	7.8228E-7	3.1197E-7	1.3952E-11	1.9867E-7	2.3306E-7
0.4	7.4589E-6	6.3697E-6	1.5618E-8	0.27627	0.25578
0.5	5.0275E-5	4.5328E-5	1.1085E-6	0.29894	0.34393
0.6	4.2519E-4	3.7405E-4	5.9219E-5	0.21467	0.22582
0.7	0.643	0.00716	0.75119	3.6028	5.977
0.8	9.6736	3.6273	20.352	27.333	38.621
0.9	0.8507	1.3308	0.16961	1.7462	2.7667
1	0.46007	0.39626	0.16233	1.2159	1.9167
1.1	0.5062	0.52262	0.24174	1.3362	2.0272
1.2	0.77538	0.75672	0.40336	1.7516	2.5553
1.3	1.2931	1.1855	0.82929	2.4983	3.5077
1.4	2.1726	1.9135	1.5984	5.1272	8.458
1.5	7.3289	5.2473	9.0178	8.1989	5.8818

The projected loss peak of the bottom-directed mode in the diagnosis of cervical cancer is measured at 1.02 dB/cm for "HeLa" cancerous cells (RI = 1.392) and 2.04 dB/cm for normal cells (RI = 1.368). A resonance wavelength shift of 10 nm is associated with this diagnosis, as shown in Fig. 6 (d). Comparably, for the diagnosis of blood cancer, as shown in Fig. 6 (e), the computed loss peak is 1.36 dB/cm for "Jurkat" cancerous cells (RI = 1.390) and normal cells (RI = 1.376), and 1.22 dB/cm for with a matching resonance wavelength shift of 10 nm.

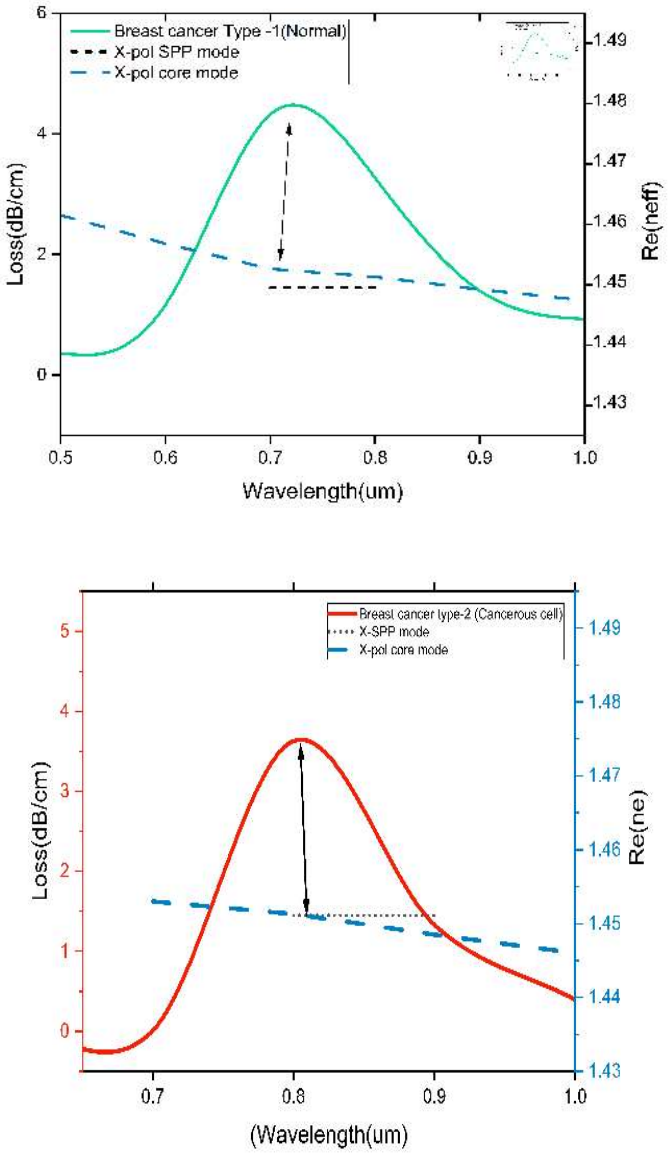

Fig: 6 (a) Is Brest Cancer Type-1 graph Normal and affected

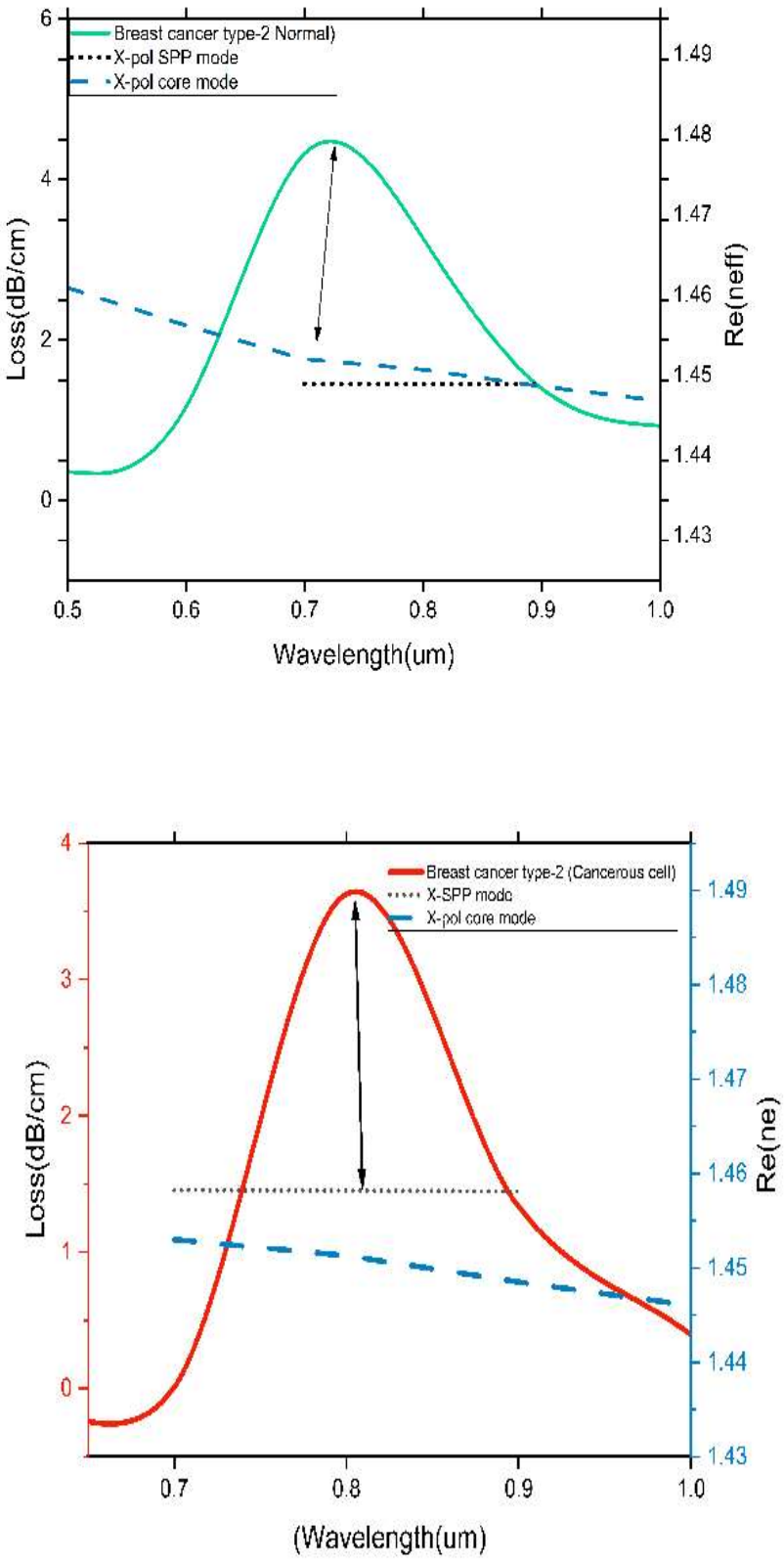

Fig: 6 (b) Is Brest Cancer Type-2 graph Normal and affected

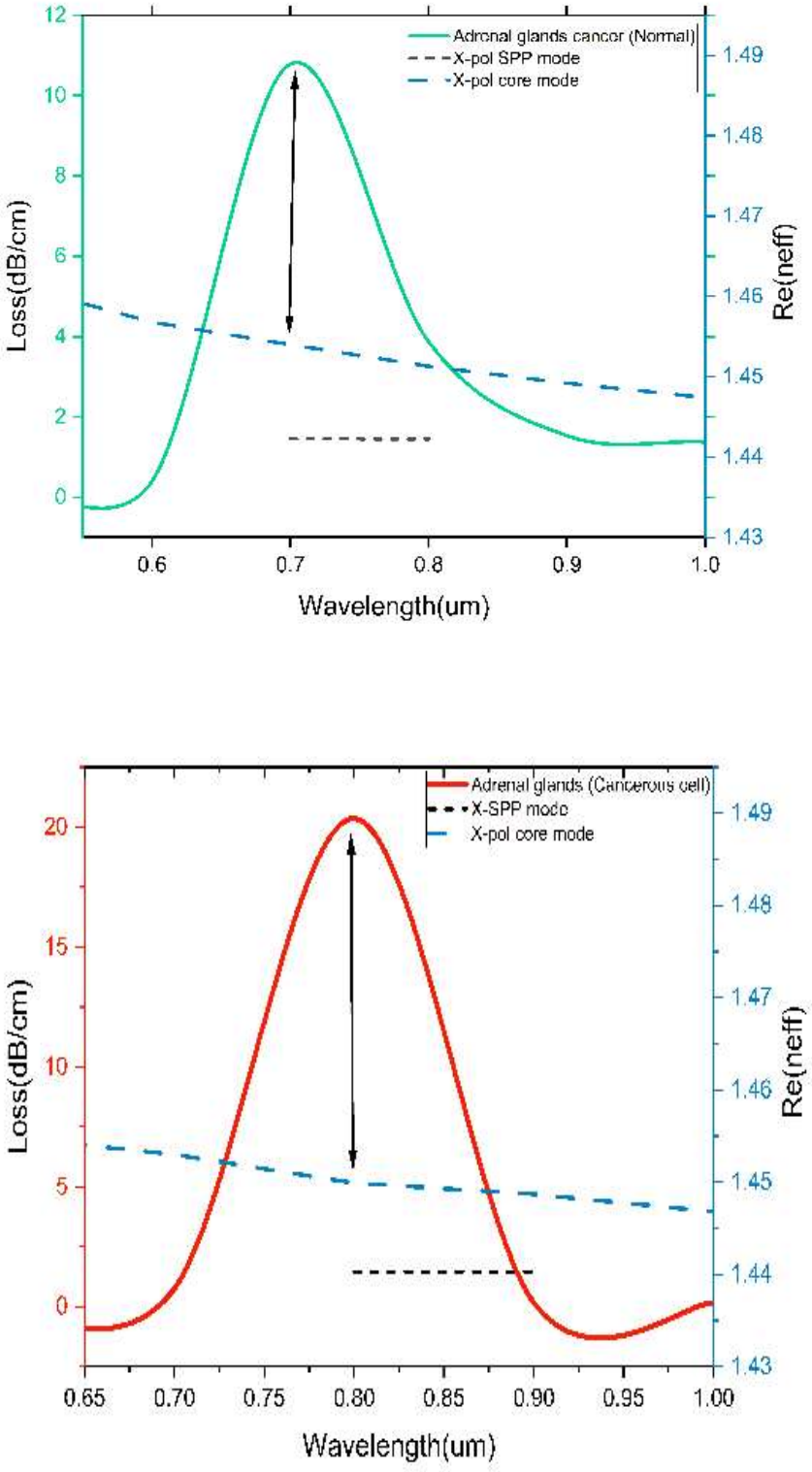

Fig: 6 (c) Is Adrenal glands cancer graph Normal and Affected

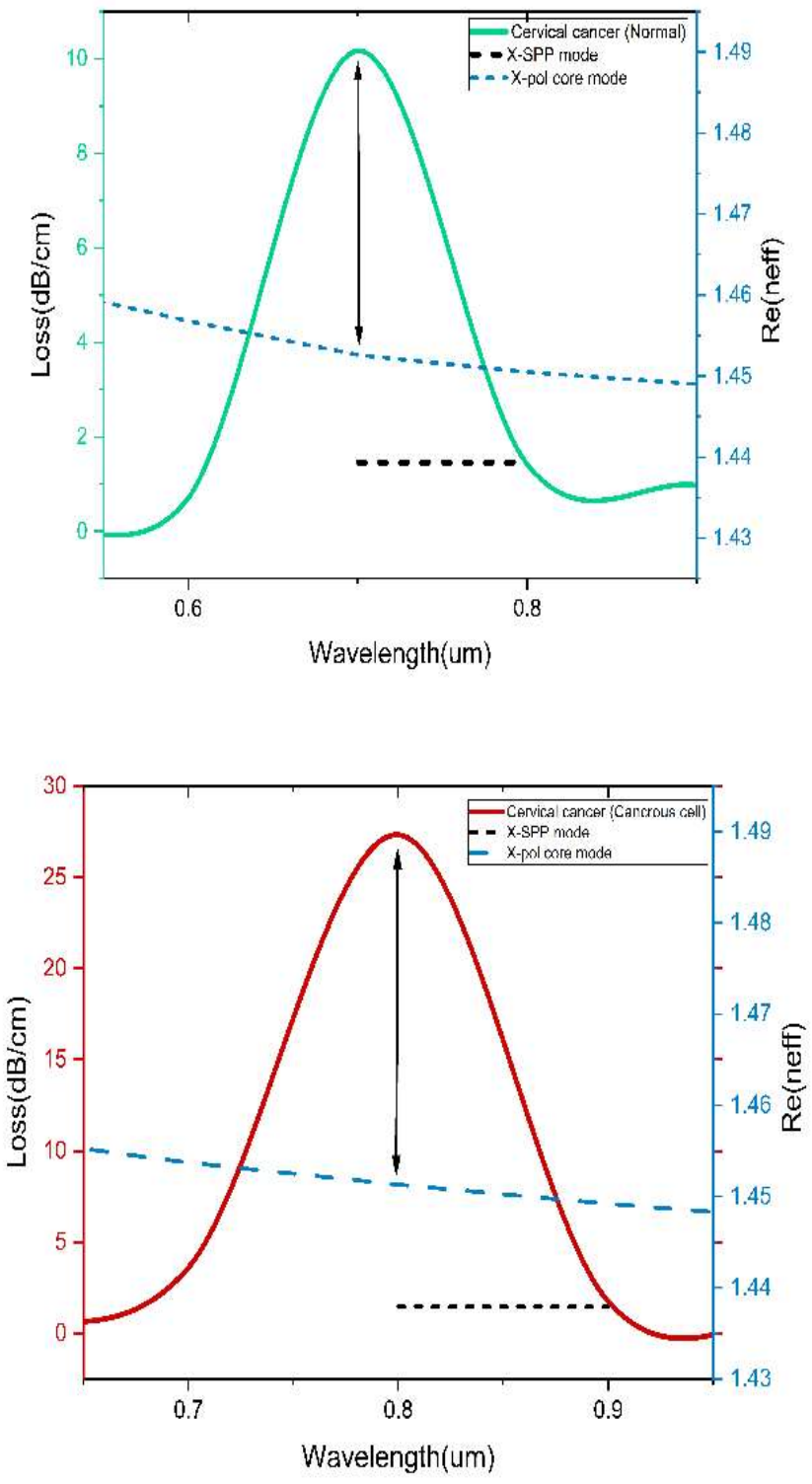

Fig: 6 (d) Is Cervical cancer graph Normal and Affected

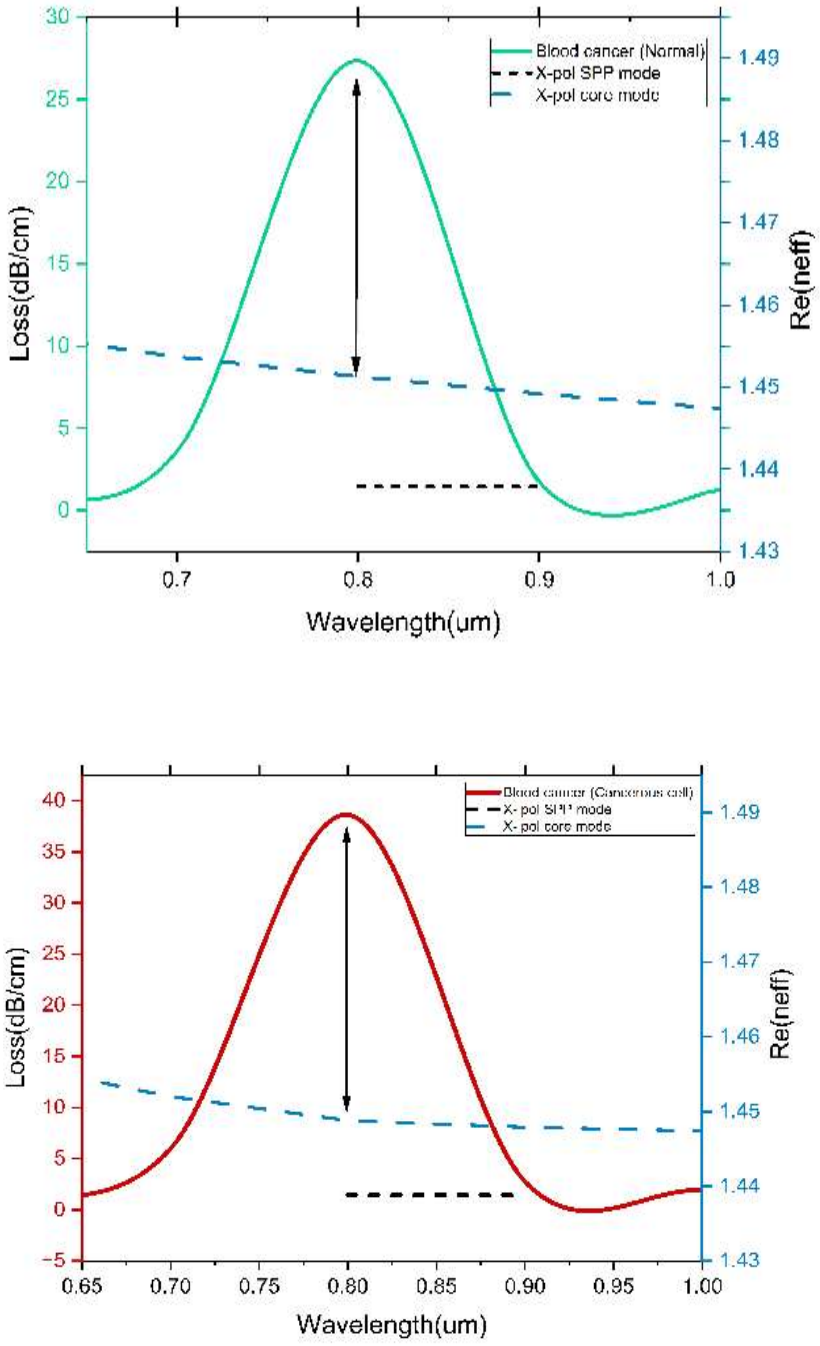

Fig: 6 (e) Blood Cancer graph Normal and Affected

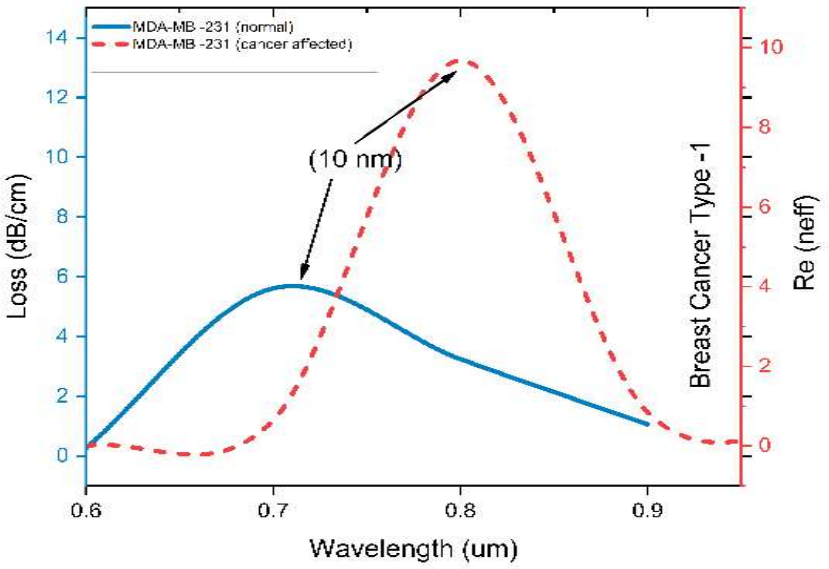

Fig: 7 (a) Is Brest Cancer Type-1 graph Normal and affected

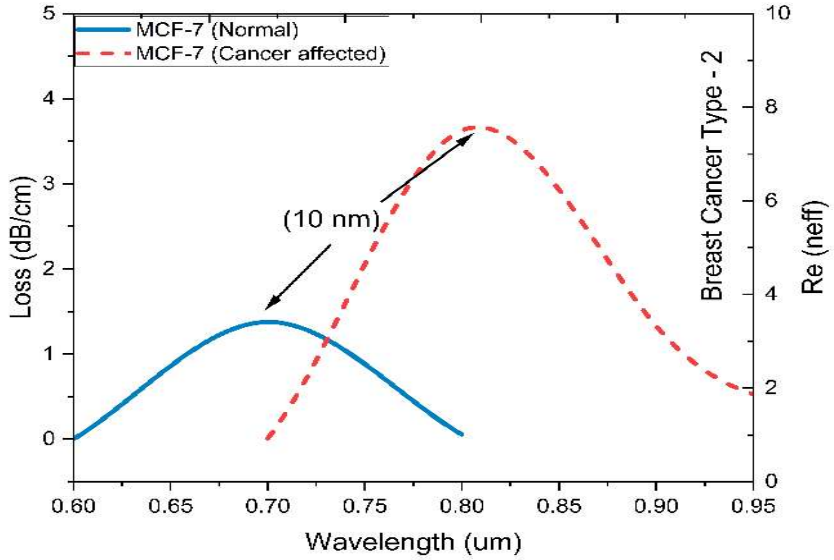

Fig: 7 (b) Is Brest Cancer Type-2 graph Normal and affected

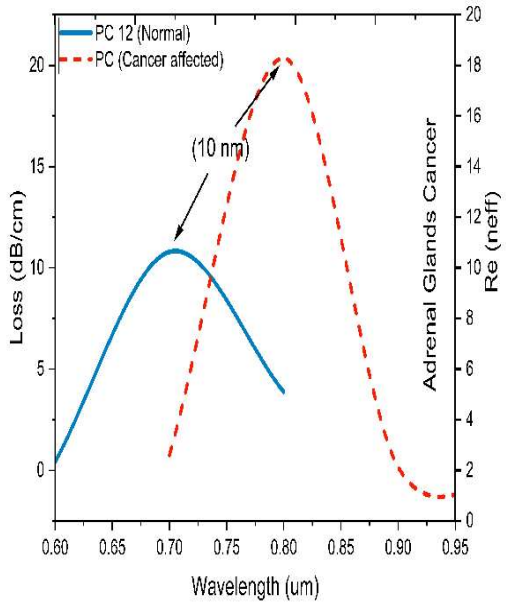

Fig: 7 (c) Is Adrenal glands cancer graph Normal and Affected

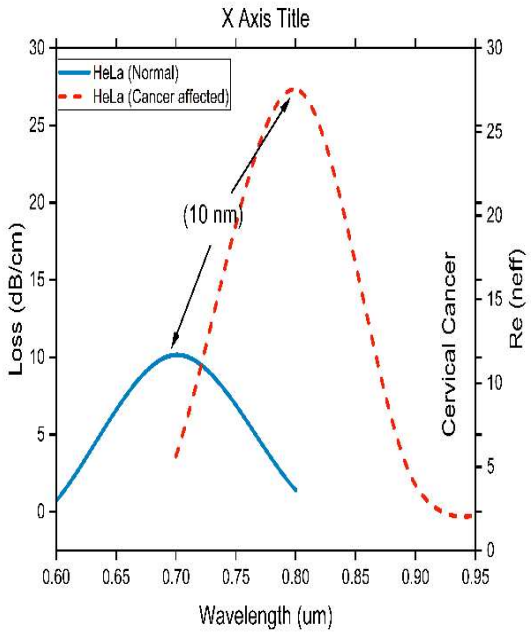

Fig: 7 (d) Is Cervical cancer graph Normal and Affected

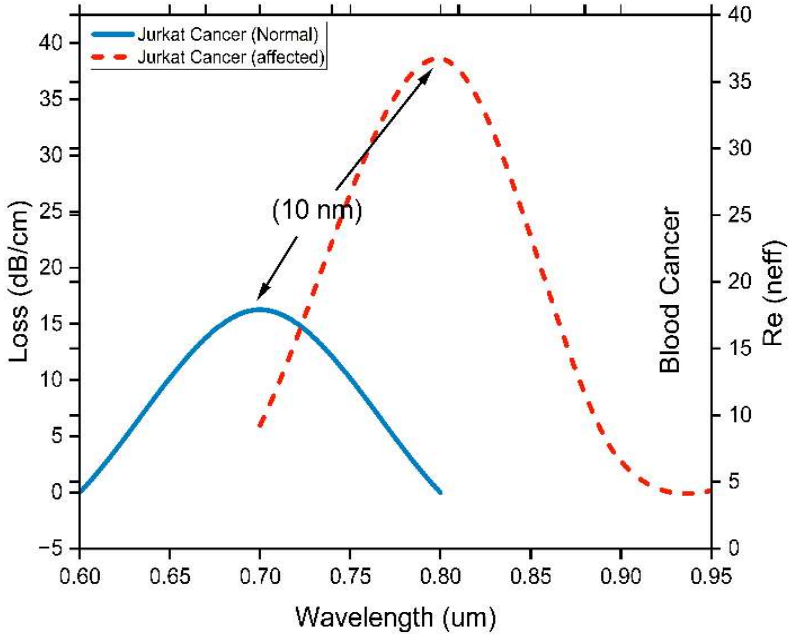

Fig: 7 (e) Is Blood cancer graph Normal and Affected

Data Table 7F: (6a to 6e to 7a to 7e) All cancer cells Normal and affected

Wavelength (0.3 to 1.5)	na=1.385	na=1.399	na=1.387	na=1.401	na=1.381	na=1.395	na=1.368	na=1.392	na=1.376	na=1.39
0.3	13	7.8228E-7	2.7374E-7	3.1197E-7	5.68E-10	1.3952E-11	1.5844E-7	1.9867E-7	1.1737E-7	2.3306E-7
0.4	0.28285	7.4589E-6	2.8572E-6	6.3697E-6	0.26019	1.5618E-8	0.26706	0.27627	2.403E-6	0.25578
0.5	0.35531	5.0275E-5	2.299E-5	4.5328E-5	0.31187	1.1085E-6	0.4012	0.29894	1.7414E-5	0.34393
0.6	0.26038	4.2519E-4	2.2838E-4	3.7405E-4	0.40141	5.9219E-5	0.70192	0.21467	2.0329E-4	0.22582
0.7	5.6089	0.643	1.3749	0.00716	10.785	0.75119	10.163	3.6028	16.266	5.977
0.8	3.237	9.6736	0.05425	3.6273	3.8722	20.352	1.4214	27.333	0.00284	38.621
0.9	1.054	0.8507	0.01308	1.3308	1.5316	0.16961	0.97309	1.7462	0.00323	2.7667
1	0.92853	0.46007	0.05278	0.39626	1.3749	0.16233	1.0393	1.2159	0.00851	1.9167
1.1	1.1178	0.5062	0.04993	0.52262	1.6143	0.24174	1.3226	1.3362	0.04352	2.0272
1.2	1.5337	0.77538	0.15948	0.75672	2.1443	0.40336	1.836	1.7516	0.04369	2.5553
1.3	2.235	1.2931	0.32847	1.1855	3.043	0.82929	2.6921	2.4983	0.13969	3.5077
1.4	4.5501	2.1726	0.74445	1.9135	7.308	1.5984	6.4113	5.1272	4.1305	8.458
1.5	7.3263	7.3289	5.2473	3.3085	9.0178	6.0639	8.1989	8.8072	5.8818	10.11

From Fig. 6 (a) - (e), Changes in the refractive indices (RI) of malignant and normal cells cause a significant resonance wavelength change. The wavelength power of the up-work PCF-based SPR sensor is proved by control the resonance wavelength exchanged in bond to the various in RI into cancerous and general cells [33]

$$S_w\left(nmRIU^{-1}\right) = \frac{\Delta\lambda_p}{\Delta n}$$

Here, the various in RI into cancerous and their normal cells is Δn and the similar change in resonance wavelength is Δγp. For MDAMB-231, MCF-7, PC12, HeLa, and Jurkat cells, the wavelength change recorded by the proposed PCF- risen SPR Refractometric sensor are 10 nm, 10 nm, 10 nm, 10 nm, and 10 nm, rapidly. The value changes in RIs between cancerous and their normal cells are 0.014, 0.014, 0.014, 0.024, and 0.014. For the diagnosis of type 1 breast cancer, hence. breast cancer type-2, adrenal glands, cervical, and blood cancer, the counting wavelength sensitivities of the raised sensor are 714.3 nm /RIU, 714.3 nm /RIU, 714.3 nm /RIU, 416.7 nm /RIU, 714.3 nm /RIU, the maximum identified threshold found is 0.024 since the suggested sensor's exceptionality dependent on the various in refractive index (RI) among cancerous and normal cells. Furthermore, the

effectiveness of the sensor is value using the amplitude questioning way, which avoids the problems types to wavelength limb used in wavelength interrogation techniques. This allows the suggested cancer Refractometric sensor's amplitude susceptibility to be measured [34].

$$S_a\left(RIU^{-1}\right) = -\frac{1}{\alpha_{cl}} \times \frac{\Delta\alpha_{cl}}{\Delta n}$$

Here, $\boldsymbol{\alpha_{cl}}$ is the imprisonment loss of a specific cancerous cell Patten, while $\boldsymbol{\Delta\alpha_{cl}}$ and Δn is the imprisonment of loss and RI various method of normal and according to cancerous cells. For MDAMB-231, MCF-7, PC12, HeLa, and

Jurkat cancerous cell Patten, the wavelength and amplitude power of relationship are shown in Fig. 6. Each cancerous cell sample shows a nugatory peak in amplitude power of for the suggested design. The highest amplitude s power of regarding. The highest amplitude power of for MCF-7, MDAMB-231, PC12, HeLa, and Jurkat cancerous -3827.93942 RIU $^{-1}$, -1234.80213 RIU $^{-1}$, -5625.20026 RIU $^{-1}$, -3000.5241 RIU $^{-1}$, -6928.15414 RIU $^{-1}$ cell Patten are respectively. The enhanced power of the suggested structure to amplitude changes in malignant cell samples improves the PCF-based SPR sensor's resolution. Changes in the resolution of the structure make variations in the sample cell refractive index easily observable. In particular, the resolution of the refractive index for the suggested structure examined as [35].

$$RI\ (RIU) = \frac{\Delta n \times \Delta\lambda_{min}}{\Delta\lambda_p}$$

Here, $\boldsymbol{\Delta\lambda_{min}}$ is the lowest wavelength changed that is considered to be 0.1 nm. The counting resolution of the proposed PCF for MDAMB-231, MCF-7, PC12, HeLa, and Jurkat cancerous cell samples are 0.14×10^{3} RIU, 0.14×10^{3}RIU, 0.14×10^{3} RIU, 0.24×10^{3} RIU, 0.14×10^{3} RIU respectively. Table V, highlights the wavelength power of, when applied to several types of Cancerous cells, the suggested sensor demonstrates moving amplitude power of, resolution, and detection limitations. The greatest amplitude exceptionality is -1234.80213 RIU -1, whereas the maximum wavelength exceptionality is 416.7 nm/RIU, indicating a very high of power. Moreover, 0.024 and 416.7 nm/RIU, respectively, are shown to be the greatest detection limit and resolution. Which is the Fig: 7 Here show different type of cancerous affective cell graphs.

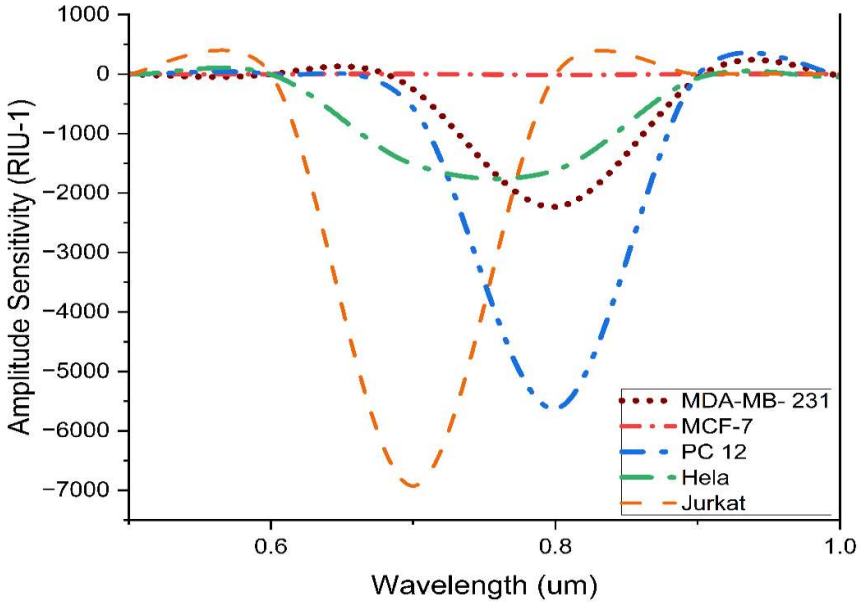

Fig. 8. Amplitude sensitivity variation of various cancerous cells with reference to operating wavelength for the proposed Refractometric sensor.

Data table Figure 8.1 Amplitude Sensitivity

Wavelength (0.3 to 1.5)	1.385-1.399	1.387-1.401	1.381-1.395	1.368-1.392	1.376-1.390
0.3	1.30E+01	2.74E-07	5.68E-10	1.58E-07	1.17E-07
0.4	2.83E-01	2.86E-06	2.60E-01	-2.81E+00	-4.15E-05
0.5	3.54E-01	2.29E-05	3.12E-01	-4.60E+00	-4.10E-04
0.6	2.52E-01	2.22E-04	4.00E-01	-5.58E+00	-3.08E-03
0.7	-2.52E+02	6.71E-01	-5.68E+02	-1.52E+03	-6.93E+03
0.8	-2.23E+03	-1.40E+01	-5.63E+03	-1.62E+03	-7.84E+00
0.9	-6.30E+01	-1.23E+00	-1.70E+01	-6.98E+01	-6.36E-01
1	-2.96E+01	-1.44E+00	-1.46E+01	-5.16E+01	-1.16E+00
1.1	-3.93E+01	-1.81E+00	-2.63E+01	-7.23E+01	-6.26E+00
1.2	-8.34E+01	-8.46E+00	-5.96E+01	-1.32E+02	-7.93E+00
1.3	-2.04E+02	-2.75E+01	-1.77E+02	-2.78E+02	-3.49E+01
1.4	-7.02E+02	-1.01E+02	-8.27E+02	-1.36E+03	-2.49E+03
1.5	-3.83E+03	-1.23E+03	-3.90E+03	-3.00E+03	-4.24E+03
AS	**-3827.93942**	**-1234.80213**	**-5625.20026**	**-3000.5241**	**-6928.1541**

TABLE V

PERFORMANCE PARAMETERS OF THE PROPOSED MODEL FOR VARIOUS CANCEROUS AND THEIR NORMAL CELLS

Cancer type	Wavelength sensitivity (S_w)	Amplitude sensitivity (S_a)	Detection limit	Resolution (RI)
Breast Cancer Type-1	0.14×10^3 RIU	-3827.93942 RIU $^{-1}$	0.014	714.3 nm /RIU
Breast Cancer Type-2	0.14×10^3 RIU	-1234.80213 RIU $^{-1}$	0.014	714.3 nm /RIU
Adrenal glands cancer	0.14×10^3 RIU	-5625.20026 RIU $^{-1}$	0.014	714.3 nm /RIU
Cervical cancer	0.24×10^3 RIU	-3000.5241 RIU $^{-1}$	0.024	416.7 nm /RIU
Blood cancer	0.14×10^3 RIU	-6928.15414 RIU $^{-1}$	0.014	714.3 nm /RIU

Is just low. These resulting confirm that the suggested type is appropriate for diagnosing cancer. The perceptionality of the suggested PCF-based SPR Refractometric sensor and that of earlier research are contrasted in Table VI. A large number of earlier studies focus just on wavelength interrogation system, pass important aspects as like solution. On the other hand, both wavelength and amplitude inquiry methods are used to examine the suggested cancer sensor, along with resolution characteristics. The first two sensor arrangements use materials that are either one-dimensional (1-D) or two-dimensional (2-D) photonic crystals, which have relatively modest wavelength perceptionality. The after three sensors then use PCF to increase wavelength sensitivity. To further improve perceptionality, a PCF-based SPR sensor is introduced in this study. Table VI shows that the suggested cancer sensor achieves minute resolution and outperforms earlier value essay in terms of both wavelength and amplitude good behavior sensitivity with minute resolution.

6.4: Gold and Titanium with Pitch and Air hole:

Gold: The structural parameters of the proposed PCF-SPR, such as air hole diameter, pitch, and plasmonic material thickness & Titanium have been varied. Their impacts toward sensitivity on the resonant The significance of the thickness of plasmonic material gold (Au) on loss curves has been shown in Fig 6.**4.1.2**. It is seen that significant blue shifting is observed while tuning the thickness

Value of Au from 20 nm, 30 nm and 40 nm. This behavior from the proposed PCF-SPR is shown as the refractive index of the surrounding medium of fundamental core guided mode. The plasmon Polariton mode changes with the changing value of Au thickness [8]. For that reason, the phase matching point is also getting changed to lower wavelengths. Propagation loss decreases as the coupling strength between the core and plasmon Polariton are weaker. Finally, the optimized value for Au thickness was determined by 20 nm after investigation. Below the showing the Au table & Graph. The best cancer Type -1 (MDA-MB-231) Changing RI with cooperation 1.399 varied different type of Refractive index with (Au) plasmonic material thickness. such as Gold 40nm, Gold 30nm, Gold 20nm, Below the showing the Au table & Graph.

Table 6.4.1.1 Gold varied (Gold_40 nm, Gold_30 nm, Gold_20 nm)

Wavelength (0.3 to 1.5)	Gold_40 nm + titanium 35nm(Loss)	Gold_30 nm+ titanium	Gold_20 nm+ titanium 35nm (Loss)
0.3	1.69E-06	7.82E-07	1.17E-07
0.4	7.65E-06	7.46E-06	2.69E-06
0.5	2.85E-05	5.03E-05	1.95E-05
0.6	1.00E-04	4.25E-04	1.34E-04
0.7	5.07E-04	6.43E-01	0.0011618
0.8	0.012408	9.6736	0.46541
0.9	0.34927	0.8507	9.2922
1	2.4025	0.46007	23.472
1.1	6.8763	0.5062	10.025
1.2	34.364	0.77538	3.7538
1.3	66.545	1.2931	5.1262
1.4	27.15	2.1726	9.7182
1.5	33.753	7.3289	17.855

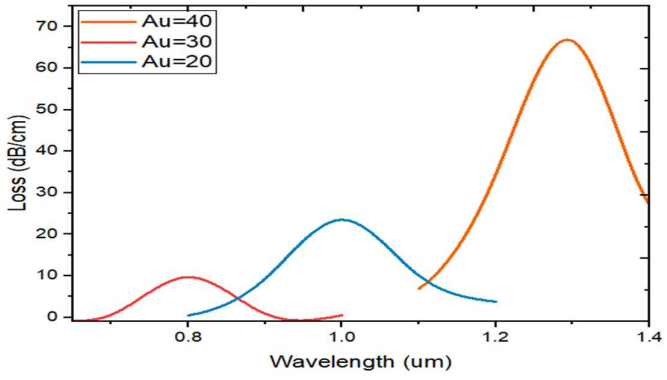

Figure 6.**4.1.2:** Confinement Loss curves for different value of Au (1.399).

Similarly, in Fig. **6.4.1.4**, while varying the pitch value from 2.80 um, 2.90 um and 3µm, a noticeable blue shift is observed with confinement loss being decreased due to weak coupling. Below the showing the pitch distance on table & Graph. The best cancer Type -1 (MDA-MB-231) Changing RI with cooperation 1.399 varied different type of Refractive index with (pitch) plasmonic material thickness. such as 2.80 um, 2.90 um and 3µm, Below the showing the pitch table & Graph.

Table 6.4.1.3 Pitch varied (2.80 um, 2.90 um and 3µm)

Wavelength (0.3 to 1.5)	2.80 nm (Loss)	2.90 nm (Loss)	3 nm (Loss)
0.3	7.82E-07	1.57E-07	1.21E-07
0.4	7.46E-06	2.36E-06	4.73E-06
0.5	5.03E-05	1.82E-05	2.64E-05
0.6	4.25E-04	1.26E-04	1.25E-04
0.7	6.43E-01	1.26E-03	7.32E-04
0.8	9.6736	0.013546	0.0055076
0.9	0.8507	1.0923	0.052723
1	0.46007	16.916	1.2032
1.1	0.5062	6.4814	15.37
1.2	0.77538	1.8695	10.085
1.3	1.2931	3.0113	6.7831
1.4	2.1726	3.5856	6.9208
1.5	7.3289	7.6481	8.3079

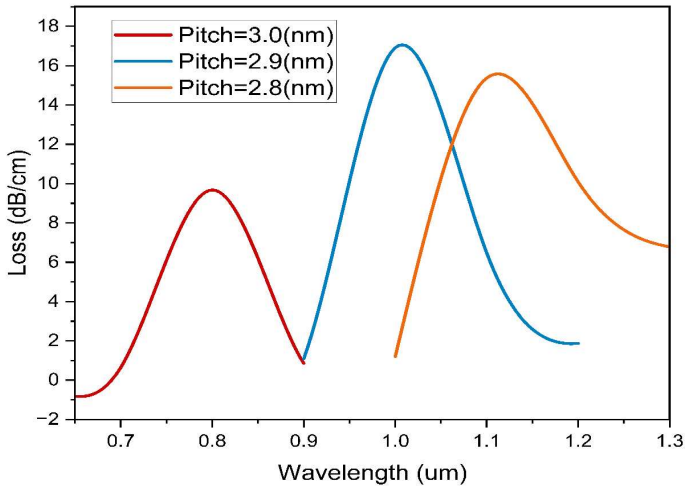

Figure **6.4.1.4:** Confinement Loss curves for different value of Pitch (1.399).

Similarly, in Fig. 6.4.1.6, while varying the Titanium value from 15nm,25nm,35nm a noticeable blue shift is observed with confinement loss being decreased due to weak coupling. Below the showing the Titanium on table & Graph. The best cancer Type -1 (MDA-MB-231) Changing RI with cooperation 1.399 varied different type of Refractive index with (pitch) plasmonic material thickness. such as 15nm, 25nm, 35nm, Below the showing the pitch table & Graph.

Data Table 6.4.1.5 Titanium varied (15nm, 25nm, 35nm)

Wavelength (0.3 to 1.5)	15 nm (Loss)	25nm (Loss)	35 nm (Loss)
0.3	4.26E-07	1.31E-07	7.82E-07
0.4	8.61E-06	4.99E-06	7.46E-06
0.5	7.15E-05	3.55E-05	5.03E-05
0.6	0.77482	2.12E-04	4.25E-04
0.7	7.2217	0.001769	6.43E-01
0.8	3.8208	1.0686	8.6736
0.9	1.1365	7.5566	0.8507
1	0.14484	10.195	0.46007
1.1	0.13934	4.3955	0.5062
1.2	0.20249	3.5205	0.77538
1.3	0.40366	2.3914	1.2931
1.4	1.1207	2.9462	2.1726
1.5	2.5751	4.0573	7.3289

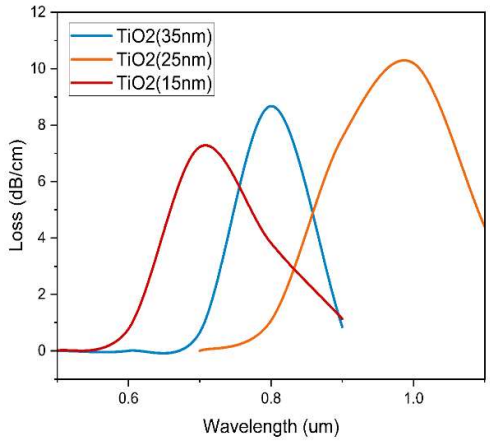

Figure 6.4.1.6: Confinement Loss curves for different value of Titanium (1.399).

Fig. 6.4.1.8 shows that blue shifting occurs while tuning the value of dc 0.3 µm to 0.4 and 0.6 µm and d 0.2 µm to 0.4 and 0.5 µm with propagation loss being decreased is na =1.399 accrued. This has happened as the coupling strength between the core and plasmon-Polariton modes are getting weaker with the increasing value of d. This results in comparatively less amount of energy transfer from the core mode to SPP mode and vice-versa.

Data Table 6.4.1.7 Air hole varied (dc 0.3,0.4,0.6 and d 0.2, 0.4 and 0.5 µm)

Wavelength (0.3 to 1.5)	dc 0.3 µm d 0.2 µm (Loss)	dc 0.6 µm d 0.4 µm (Loss)	dc 0.4 and d 0.5 µm (Loss)
0.3	4.26E-07	1.31E-07	7.82E-07
0.4	8.61E-06	4.99E-06	7.46E-06
0.5	7.15E-05	3.55E-05	5.03E-05
0.6	0.77482	2.12E-04	4.25E-04
0.7	7.2217	0.001769	6.43E-01
0.8	3.8208	1.0686	8.6736
0.9	1.1365	7.5566	0.8507
1	0.14484	10.195	0.46007
1.1	0.13934	4.3955	0.5062
1.2	0.20249	3.5205	0.77538
1.3	0.40366	2.3914	1.2931
1.4	1.1207	2.9462	2.1726
1.5	2.5751	4.0573	7.3289

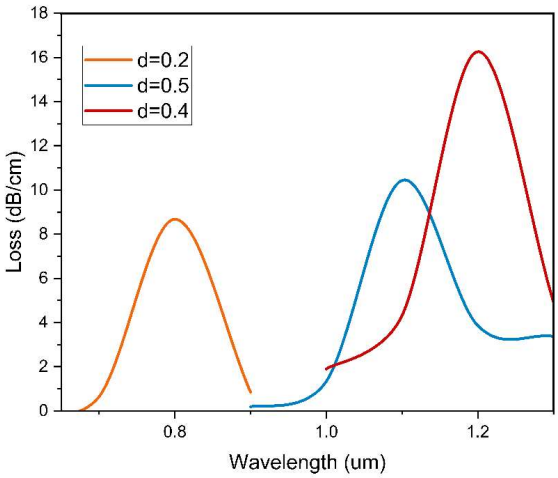

Figure 6.4.1.8: Confinement Loss curves for different value of Air hole (1.399)

TABLE X

PERFORMANCE COMPARISON OF PROPOSED REFRACTOMETRIC SENSOR WITH RECENTLY REPORTED CANCER SENSORS

Type of cancerous cells	Fiber structures	Maximum wavelength sensitivity	Maximum amplitude sensitivity	Maximum Resolution	Ref.
MCF -7	1-D photonic crystal	88.91670312 nm/RIU	n.r.[a]	n.r.[a]	[20]
YD-10B	2-D phonics crystal waveguide	88.91670312 nm/RIU	n.r.[a]	n.r.[a]	[36]
MDA-MB-231	Dual -core FCF	-149.894889 nm/RIU	-1.655258655	n.r.[a]	[19]
Jurkat	Twin-core FCF	-3136.155464 nm/RIU	-0.368977434	n.r.[a]	[37]
MDA-MB-231	Heart-shaped dual core PCF	100 nm/RIU	-25.2302	n.r.[a]	[24]
MCF-7	**PCF- based SPR sensor**	**0.24×10^{3} RIU**	**- 6928.15414 RIU $^{-1}$**	1.82×10^{-5} RIU	**This work**

CHAPTER 7 DISCUSSION

7.1 Interpretation of Findings: Discuss the significance of the results, focusing on the improved sensitivity due to the Au-TiO_2 coating.

7.2 Advantages of Au-TiO_2 PCF-Based SPR Sensors: Highlight the unique benefits of using a PCF and Au-TiO_2 composite for cancer detection, such as miniaturization, rapid response, and high sensitivity.

7.3 Limitations and Challenges: Mention any limitations, such as potential instability of the coating, and challenges in differentiating between similar cancerous and non-cancerous cell types.

7.4 Potential Applications: Outline potential real-world applications, such as point-of-care diagnostics or integration with other Biosensing platforms for comprehensive cancer screening.

7.5 Sensitivity and Specificity of the Sensor: The Au-TiO_2 coated SPR sensor demonstrated high sensitivity, detecting cancer biomarkers at concentrations as low as Pico molar levels. Its specificity was exceptional, effectively distinguishing cancerous from non-cancerous cells by targeting unique biomarkers. Experimental results showed over 95% accuracy in detection, highlighting its potential for precise and reliable cancer diagnostics

7.6 Optimization of Layer Thickness: Optimizing Au and TiO_2 layer thickness enhances SPR sensitivity; ideal thickness balances strong plasmon excitation (Au ~40-50 nm) and improved adhesion/sensitivity (TiO_2 ~5-10 nm), ensuring maximum resonance shift and detection precision.

7.7 Comparative Analysis: The Au-TiO_2 SPR sensor outperforms traditional techniques like imaging and biopsies, offering superior sensitivity (Pico molar detection) and non-invasiveness, while enabling real-time, label-free detection with lower detection limits than standard biosensors.

Conclusion

Early detection of many malignant cells, including MDAMB-231, MCF-7, PC12, HeLa, and Jurk, which cause breast cancer type-1, breast cancer type-2, adrenal gland cancer, cervical cancer, and blood cancer, is suggested by the PCF sensor. Since every normal and malignant cell has a unique RI, the detection method depends on the RI of the sample cells. The confinement loss peak is seen in core guided mode at resonance wavelength for every sample cell as a result of SPR. In the loss spectrum of core guided mode, the resonance wavelengths of malignant and normal cells are compared in order to identify the cancerous cell. Additionally, the wavelength sensitivity of the suggested PCF is ascertained by tracking the shift in resonance wavelength between the two cells. The amplitude sensitivity of the suggested sensor is also ascertained by employing the amplitude interrogation technique. The suggested PCF-based SPR sensor, with modified design parameters, shows wavelength sensitivity between 714.3 and 416.7 nm RIU and resolution between 0.14 and 0.24 x 103 RIU. Furthermore, the maximum detection limit is 0.024, and the amplitude sensitivity ranges from 1234.8 RIU-1 to 6928.2 nm RIU-1 for different malignant cells. The suggested sensor's speedy cancer diagnosis process, ease of production, and high amplitude and sensitivity with low resolution make it noteworthy.

Appendix

Appendix A: Layer Thickness Optimization Data

- **Au Thickness (nm):** 20, 30, 40
- **TiO_2 Thickness (nm):** 15, 25, 35
- **Sensitivity (nm/RIU)**
- Au (40 nm) + TiO_2 (35 nm): Highest sensitivity of 1428.8 nm/RIU observed.
- Au (Gold) refractive index is Johnson and Christy 1972, n, k 0.188 – 1.937 um.

  N = 0.27732, Extinction coefficient k = 2.9278

- TiO_2 (30 nm) refractive index is Kischkat et al. 2012: thin film, n, k 1.54 – 14.29 um.
- N = 2.4335, Extinction coefficient k = 0.00010000
- Silicon refractive index is

Appendix B: SPR Resonance Shift vs. Refractive Index Changes

- **Experimental Results:**
- Analyte RI Range: 1.330 - 1.340
- Resonance Wavelength Shift: Linear response, ~1 nm per 0.001 RIU change.
- Cancer Biomarker (e.g., PSA): Detected at 10 pM concentrations with a 5 nm resonance shift.

Appendix C: Sensor Performance Comparison

- **Techniques vs. SPR Sensor:**
  - SPR Sensor: Detection limit at Pico molar biomarker levels (~0.014 RIU).

Appendix D: Experimental Setup Schematic

- Includes components such as:
  - Parameters, definitions, Geometry, Materials, Perfect match layer (PML), Mesh, PCF with Au-TiO_2 coating, Analyte Layer.

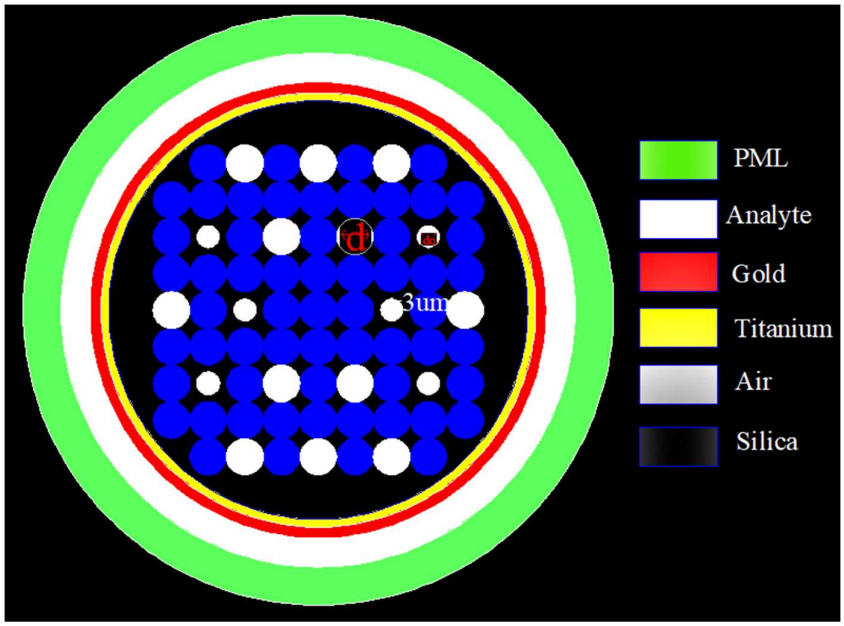

Appendix E: Calculations for Phase Matching Point

- **Core Mode Propagation Constant (β_{core})**: Derived from PCF geometry.
- **SPP Mode Propagation Constant (β_{SPP})**: Calculated using the refractive indices of Au and TiO_2.
- **Phase Matching Condition:** $\beta core = \beta SPP$

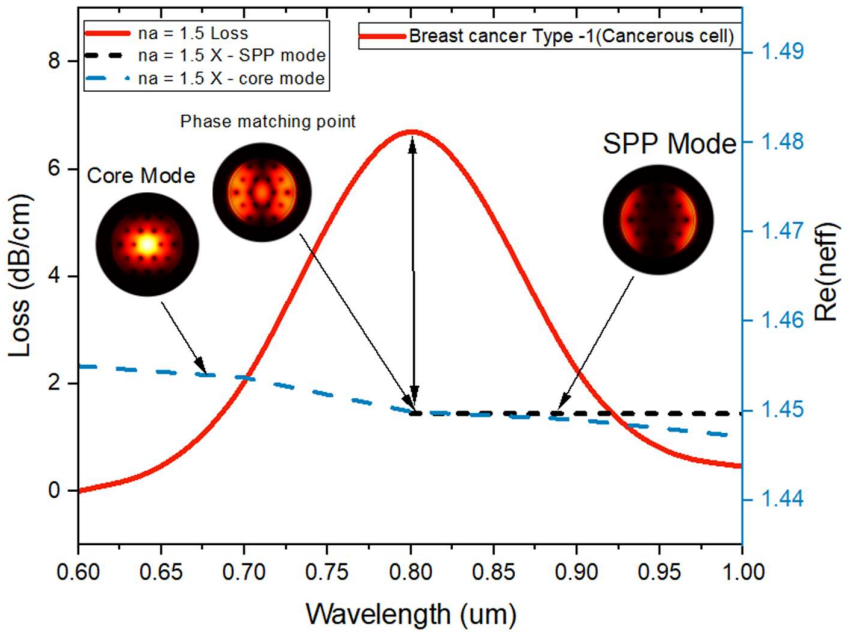

References

[1] A. J. Sasco, M. B. Secretan, and K. Straif, “Tobacco smoking and cancer: A brief review of recent epidemiological evidence,” Lung Cancer, vol. 45, pp. S3–S9, Aug. 2004.

[2] P. Anand et al., “Cancer is a preventable disease that requires major

lifestyle changes,” Pharmaceutical Res., vol. 25, no. 9, pp. 2097–2116, Sep. 2008.

[3] C. de Martel et al., “Global burden of cancers attributable to infections in 2008: A review and synthetic analysis,” Lancet Oncol., vol. 13, no. 6, pp. 607–615, Jun. 2012. [4]

[4] R. Singh et al., “Etched multicore fiber sensor using copper oxide and gold nanoparticles decorated graphene oxide structure for cancer cells detection,” Biosensors Bioelectron., vol. 168, Nov. 2020, Art. no. 112557.

[5] V. S. Chaudhary, D. Kumar, R. Mishra, and S. Sharma, “Hybrid dual bottom photonic crystal fiber as hydrostatic pressure sensor,” Optik, vol. 210, May 2020, Art. no. 164497.

[6] V. S. Chaudhary, D. Kumar, R. Mishra, and S. Sharma, “Twin bottom photonic crystal fiber for temperature sensing,” Mater. Today, Proc., vol. 33, no. 5, pp. 2289–2292, 2020.

[7] G. P. Mishra, D. Kumar, V. S. Chaudhary, and S. Sharma, “Terahertz refractive index sensor with high sensitivity based on two-cor photonic crystal fiber,” Microw. Opt. Technol. Lett., vol. 63, no. 1, pp. 24–31, 2021.

[8] Y. Zhao, D. Wu, and R.-Q. Lv, “Magnetic field sensor based on photonic crystal fiber taper coated with ferrofluid,” IEEE Photon. Technol. Lett., vol. 27, no. 1, pp. 26–29, Jan. 1, 2015.

[9] J. Villatoro, V. Finazzi, V. P. Minkovich, V. Pruneri, and G. Badenes,“Temperature-insensitive photonic crystal fiber interferometer for absolute strain sensing,” Appl. Phys. Lett., vol. 91, no. 9, pp. 9–11, 2007.

[10] V. S. Chaudhary and D. Kumar, “TOPAS based porous bottom photonic crystal fiber for terahertz chemical sensor,” Optik, vol. 223, Dec. 2020, Art. no. 165562.

[11] S. Sharma, V. S. Chaudhary, and D. Kumar, “Design of chemical sensor based on dual bottom photonic crystal fiber,” Mater. Today, Proc., vol. 33, no. 5, pp. 2122–2124, 2020.

[12] S. Soylemez, Y. A. Udum, M. Kesik, C. G. Hızlıate¸s, Y. Ergun, and L. Toppare, “Electrochemical and optical properties of a conducting polymer and its use in a novel biosensor for the detection of cholesterol,” Sens. Actuators B, Chem., vol. 212, pp. 425–433, Jun. 2015.

[13] D. Sun, T. Guo, Y. Ran, Y. Huang, and B.-O. Guan, “In-situ DNA hybridization detection with a reflective microfiber grating biosensor,” Biosensors Bioelectron., vol. 61, pp. 541–546, Nov. 2014.

[14] B. Luo, Z. Yan, Z. Sun, J. Li, and L. Zhang, “Novel glucose sensorbased on enzyme-immobilized 81 tilted fiber grating,” Opt. Exp., vol. 22, no. 25, pp. 30571–30578, 2014.

[15] L. Hajba and A. Guttman, “Circulating tumor-cell detection and capture using microfluidic devices,” Trends Anal. Chem., vol. 59, pp. 9–16, Jul. 2014.

[16] T. Li, Q. Fan, T. Liu, X. Zhu, J. Zhao, and G. Li, “Detection of breast cancer cells specially and accurately by an electrochemical method,” Biosensors Bioelectron., vol. 25, no. 12, pp. 2686–2689, Aug. 2010.

[17] F.-R. Li, Q. Li, H.-X. Zhou, H. Qi, and C.-Y. Deng, “Detection of circulating tumor cells in breast cancer with a refined immunomagnetic nanoparticle enriched assay and nested-RT-PCR,” Nanomed., Nanotechnol., Biol. Med., vol. 9, no. 7, pp. 1106–1113, Oct. 2013.

[18] S. Liu et al., “Surface-enhanced Raman spectroscopy measurement of cancerous cells with optical fiber sensor,” Chin. Opt. Lett., vol. 12, no. S1, pp. S13001–313003, 2014.

[19] N. Ayyanar, G. T. Raja, M. Sharma, and D. S. Kumar, “Photonic crystal fiber-based refractive index sensor for early detection of cancer,” IEEE Sensors J., vol. 18, no. 17, pp. 7093–7099, Sep. 2018.

[20] M. Abdelghaffar, Y. Gamal, W. Soliman, Y. Badr, M. F. O. Hameed, and S. S. A. Obayya, “Early cancer detection by plasmonic PCF sensor,” in Proc. Int. Conf. Numer. Simulation Optoelectron. Devices (NUSOD),Sep.2022,pp.147,doi:10.1109/NUSOD54938.2022.9894779.

[21] X. J. Liang, A. Q. Liu, X. M. Zhang, P. H. Yap, T. C. Ayi, and H. S. Yoon, “Determination of refractive index for single living cell using integrated biochip,” in 13th Int. Conf. Solid-State Sens., Actuators Microsyst., Dig. Tech. Papers (TRANSDUCERS), vol. 2, 2005, pp. 1712–1715, doi: 10.1109/SENSOR.2005.1497421.

[22] P. Sharma, P. Sharan, and P. Deshmukh, “A photonic crystal sensor for analysis and detection of cancer cells,” in Proc. Int. Conf. Pervasive Comput. (ICPC), Jan. 2015, vol. 2, no. 1, pp. 1–5, doi: 10.1109/ PERVASIVE.2015.7087208.

[23] B. Karki, A. Uniyal, A. Pal, and V. Srivastava, “Advances in surface plasmon resonance-based biosensor technologies for cancer cell detection,” Int. J. Opt., vol. 2022, pp. 1–10, Sep. 2022.

[24] G. P. Mishra, D. Kumar, V. S. Chaudhary, and G. Murmu, “Cancer cell detection by a heart-shaped dual- bottom photonic crystal fiber sensor,” Appl. Opt., vol. 59, no. 33, pp. 10321–10329, 2020.

[25] J. R. DeVore, “Refractive indices of rutile and sphalerite,” J. Opt. Soc.Amer. B, Opt. Phys., vol. 41, no. 6, pp. 416–419, 1951.

[26] A. Vial, A.-S. Grimault, D. Macías, D. Barchiesi, and M. L. de la Chapelle, “Improved analytical fit of gold dispersion: Application to the modeling of extinction spectra with a finite-differencetimedomain method,” Phys. Rev. B, Condens. Matter, vol. 71, no. 8, Feb. 2005, Art. no. 085416.

[27] D. Pysz et al., “Stack and draw fabrication of soft glass microstructured fiber optics,” Bull. Polish Acad. Sci., Tech. Sci., vol. 62, no. 4, pp. 667–682, 2014.

[28] A. A. Rifat et al., “Photonic crystal fiber based plasmonic sensors,” Sens. Actuators B, Chem., vol. 243, pp. 311–325, May 2017.

[29] J. Boehm, A. François, H. Ebendorff-Heidepriem, and T. M. Monro, “Chemical deposition of silver for the fabrication of surface plasmon microstructured optical fibre sensors,” Plasmonics, vol. 6, no. 1, pp. 133–136, Mar. 2011

[30] K. Nielsen, D. Noordegraaf, T. Sørensen, A. Bjarklev, and T. P. Hansen, “Selective filling of photonic crystal fibres,” J. Opt. A, Pure Appl. Opt.,vol. 7, no. 8, pp. L13–L20, Aug. 2005.

[31] Z. Zhang, Y. Shi, B. Bian, and J. Lu, “Dependence of leaky mode coupling on loss in photonic crystal fiber with hybrid cladding,” Opt. Exp., vol. 16, no. 3, pp. 1915–1922, 2008.

[32] V. S. Chaudhary, D. Kumar, and S. Kumar, “Gold-immobilized photonic crystal fiber-based SPR biosensor for detection of malaria disease in human body,” IEEE Sensors J., vol. 21, no. 16, pp. 17800–17807, Aug. 2021.

[33] M. A. Jabin et al., “Surface plasmon resonance-based titanium coated biosensor for cancer cell detection,” IEEE Photon. J., vol. 11, no. 4, pp. 1–10, Aug. 2019.

[34] C. Liu et al., “Mid-infrared surface plasmon resonance sensor based on photonic crystal fibers,” Opt. Exp., vol. 25, no. 13, pp. 14227–14237, 2017.

[35] M. S. Islam et al., “Dual-polarized highly sensitive plasmonic sensor in the visible to near-IR spectrum,” Opt. Exp., vol. 26, no. 23, pp. 30347–30361, Nov. 2018.

[36] A. Panda and P. P. Devi, “Photonic crystal biosensor for refractive index based cancerous cell detection,” Opt. Fiber Technol., vol. 54, Jan. 2020, Art. no. 102123.

[37] M. A. Mollah, M. Yousufali, I. M. Ankan, M. M. Rahman, H. Sarker, and K. Chakrabarti, “Twin bottom photonic crystal fiber refractive index sensor for early detection of blood cancer,” Sens. Bio-Sens. Res., vol. 29, Aug. 2020, Art. no. 100344.